INTERNATIONAL JOURNAL FOR NUMERICAL METHODS IN FLUIDS
Int. J. Numer. Meth. Fluids 2003; **41**:357–388 (DOI: 10.1002/fld.445)

Comparison of DES, RANS and LES for the separated flow around a flat plate at high incidence

M. Breuer[1,*,†], N. Jovičić[1] and K. Mazaev[2]

[1] *Lehrstuhl für Strömungsmechanik, Universität Erlangen-Nürnberg, Cauerstr. 4, D-91058 Erlangen, Germany*
[2] *Saint Petersburg State Marine Technical University, Lotsmanskaja Street 3, 190008 Saint Petersburg, Russia*

SUMMARY

The separated turbulent flow past an inclined flat plate with sharp leading and trailing edges was computed based on three different simulation approaches for a Reynolds number $Re_c = 20\,000$ and a high angle of attack $\alpha = 18^\circ$. The simulation techniques applied were the Reynolds-averaged Navier–Stokes (RANS) equations combined with a one-equation Spalart–Allmaras turbulence model, the large-eddy simulation (LES) based on an algebraic eddy-viscosity model, and a hybrid approach known as detached-eddy simulation (DES) applying a slightly modified Spalart–Allmaras model in the entire integration domain. DES is a non-zonal coupling technique of RANS and LES developed in the hope of reducing the large computational resources required for LES computations of turbulent flows with practical relevance. However, the objective of the present study was not to compare the resources (CPU time, memory) required for all three techniques but to investigate and evaluate the quality of the predicted results for RANS, DES and LES. For this purpose, a test case which is favourable to the basic concept of DES and which places special emphasis on the LES part of the DES concept was chosen. This last issue was important since the modified Spalart–Allmaras model applied as a subgrid scale model in the LES part is not as well validated as other models usually applied in LES. For this purpose, an LES prediction on a very fine grid served as a reference case for the evaluation. For all three techniques, predictions with different grid resolutions were carried out and compared with each other based on important integral parameters (e.g. Strouhal number, mean drag and lift coefficients and their standard deviations), the instantaneous and time-averaged flow structures, and higher-order statistics. As expected, the pure RANS calculation, although applied as unsteady RANS, failed to predict the unsteady characteristics of the separated flow. In contrast, the DES approach yielded reasonably the shedding phenomenon and some integral parameters. However, analysing the results in more detail led to remarkable deviations between the DES and LES predictions also when the same grid resolution was applied. Especially the free shear layer originating from the leading edge of the plate was not well reproduced by DES, showing strong deficiencies of the model applied as a subgrid scale model. The reasons for this behaviour of the model were analysed in detail. Two basic causes were identified; the first is given by some near-wall corrections in the finite Reynolds number version of the model which are not working properly in the LES mode of DES. The second is a modified definition of the filter width typically applied for DES, leading to strongly increased values of the eddy viscosity. A revised

* Correspondence to: M. Breuer, LSTM, Universität Erlangen–Nürnberg, Cauerstr. 4, D–91058 Erlangen, Germany.
† E-mail: breuer@lstm.uni-erlangen.de

Contract/grant sponsor: German Academic Exchange Programme (DAAD)
Contract/grant sponsor: Deutsche Forschungsgemeinschaft; contract/grant number: BR 1847/2

Received 10 June 2002
Revised 16 September 2002

version of the S–A model taking both issues seriously into account was used as a subgrid scale model in the LES mode. As a direct consequence, much better agreement with the reference LES solution was found for the DES prediction on the coarse grid, eliminating the deficiencies of the original formulation.

KEY WORDS: large-eddy simulation; detached-eddy simulation; separation; high-lift configuration

1. INTRODUCTION

It is well known that the prediction of complex separated unsteady flows based on Reynolds-averaged Navier–Stokes (RANS) is not completely successful for many cases. Unfortunately, even the use of the most modern turbulence models could not essentially improve the situation. Therefore, during the last decade many researchers have paid more attention towards large-eddy simulation (LES) and direct numerical simulation (DNS) as alternative prediction methods. However, these alternatives are actually too expensive in the sense of the required computer performance; this thesis is clear for DNS, but the situation with LES, if the development of supercomputers is taken into account, seems to be not so drastic. Nevertheless, the analysis carried out by Spalart *et al.* [1] shows that for Reynolds numbers of about 10^7, i.e. normal *aerodynamic* values, a computational grid consisting of a minimum of 10^{11} cells has to be used. Such huge computations will be out of reach for the next couple of decades. This circumstance, namely very high computational costs, was the main reason for developing new kinds of *hybrid* methods, which combine the main features of both LES and RANS simulations (see, e.g. References [2–6]). In the present work, the detached-eddy simulation (DES) hybrid approach is used, whose basic principles are described in Reference [1] and first results are presented in Reference [7]. The results of DES are compared with both RANS and LES data, all obtained by the same computer code. The main difference between other attempts at coupling RANS and LES is that the flow is not explicitly subdivided into two zones. As a consequence, there is no problem of explicit boundary conditions between RANS and LES zones. The main features of DES and the differences between LES, DES and RANS simulations are discussed below.

In spite of the widespread application of RANS predictions for turbulent flows, the main disadvantage of the method is clear: RANS describes flows in a statistical sense typically leading to time-averaged pressure and velocity fields. Generally, this approach is not able to distinguish between quasi-periodic large-scale and turbulent chaotic small-scale features of the flow field. This leads to huge problems when the flow field is governed by both phenomena. A typical representative is a bluff-body flow. Generally, the RANS approach is not able to reproduce the unsteady characteristics of the flow field reasonably, resulting in an inadequate description of unsteady phenomena, such as vortex formation and shedding behind bluff or inclined bodies. Even with help of complex turbulence models which are usually semi-empirical and contain about 6–9 empirical constants, it is not possible to model these large-scale phenomena adequately. LES, on the other hand, operates with unsteady fields of physical values; the governing equations are the Navier–Stokes equations but, unlike the RANS approach, spatial filtering is applied instead of averaging in time, and turbulent stresses are divided into resolved and modelled stresses. The latter can be found from very simple (in comparison with the *normal* turbulence models) subgrid scale models, often based on an

algebraic eddy-viscosity concept such as Smagorinsky's hypothesis [8]. As mentioned above, the main disadvantage of LES is the high computational costs resulting from extremely fine grids used for the direct prediction of the *non-modelled* vortical structures. Additionally very fine time steps are required for resolving the turbulent time scales.

DES could be represented as a *natural* hybrid method combining RANS and LES (see Section 3). This means, that near solid boundaries the governing equations *work* in the RANS mode, i.e. all turbulent stresses should be modelled with the help of a statistical turbulence model such as the Spalart–Allmaras (S–A) model [9]. Furthermore, pressure and velocity fields are time averaged and unsteady attached vortical structures should not be resolved directly. Far from solid boundaries, the method *switches* to the LES mode. From the physical point of view, it means resolving all large-scale vortical structures and modelling of small eddies based on a subgrid scale model, which can be similar to a statistical turbulence model. From the numerical point of view, one has to deal with unsteady fields of pressure and velocity in this mode. However, the computational domain contains no explicit boundaries or interfaces between the two modes of operation. It is natural that RANS *works* within the attached boundary layer region, where statistical turbulence models in general perform properly. Moreover, LES is applied far from the boundaries in the detached flow region, where large unsteady vortices, which should be resolved directly, are present. Exactly this kind of division allows us to use a coarse, highly stretched grid near the walls for the RANS simulation unlike in LES which requires a fine resolution in all three spatial directions. Furthermore, the spanwise and streamwise resolution do not have to be very high for RANS [10]. Both factors raise the hope that DES can be used with acceptable effort even for high Reynolds numbers, typically encountered in technical applications.

Therefore, the main application area of DES should be in accordance with the DES concept itself: unsteady turbulent flows with large separation regions for which RANS predictions do not work properly. DES modelling of non-separated flow typically leads to severe problems, as demonstrated by Nikitin *et al.* [10]. For a plane channel flow the predicted results were stable up to very high Reynolds numbers, and can be obtained even on very coarse grids. However, both constants in the logarithmic law of the wall were strongly overpredicted compared with classical values; the authors explained this as being due to both insufficient grid resolution and a non-adjusted Spalart–Allmaras model [9] (because the S–A model was originally developed for RANS only). It should be mentioned that usually DES works purely in RANS mode if the flow does not separate [7]; otherwise, some kind of initial velocity perturbations should be used in order to induce the unsteady mode as shown for the channel test case [10]. On the other hand, all DES applications of separated flows briefly summarized below were successful. Hence DES applications to such turbulent flows seem to be reasonable and reliable whose dynamics are defined by large-scale separated vortices playing a dominant role in the energy balance.

For a brief review of published papers dedicated to DES, both the steps of its development and some basic advantages of this new approach are considered. Spalart *et al.* [1] formulated the principles of DES and derived the DES constant C_{DES} based on the simulation of homogeneous turbulence, which controls the switching process between RANS and LES. Thus, DES was adjusted; furthermore, the first true (three-dimensional) simulation was applied to the flow around an NACA wing profile [7] for a very wide range of angle of attacks ($0^\circ \leqslant \alpha \leqslant 90^\circ$). For the high (from the point of view of DNS/LES) Reynolds number of about 10^5 results were obtained which were in very good agreement with experimental investigations and much

better than those obtained by pure RANS. Forsythe *et al.* [11] made the first attempt to use DES on an unstructured grid; it was shown that the C_{DES} value has to be adapted because of the special shape of the grid cells. The DES solution was found to be much more reliable than the RANS result for each of the two turbulence models used.

A classical test case for LES, namely the flat channel flow, was investigated by Nikitin *et al.* [10]. In spite of some problems with the constants in the predicted logarithmic mean velocity profile already mentioned above, the simulations were at least partially successful: the solution was stable over a very wide range of *Re* and almost does not depend on the grid resolution, which was much coarser than typically needed for LES. Here some demands on the grid are given:

- the first grid layer near the boundary should correspond to a non-dimensional value $y^+ \sim 1$ (thus, no wall-functions are required);
- a stretching ratio of about 1.15 could be used (the authors [10] deduced that only 17 additional grid layers would be necessary if the Reynolds number were to be increased by one order of magnitude);
- the non-dimensional size of the grid cells in both the longitudinal and spanwise directions (x^+ and z^+) is several orders of magnitude larger than the normal size.

An investigation of another classical test case, the flow around a circular cylinder, by Travin *et al.* [12] shows some possible problems: although the values of the base pressure, the friction coefficient, the total drag and the vortex shedding frequency were very close to the experimental values, at the same time the estimated error for the length of the recirculation zone and for the turbulent stresses was very large. Nevertheless, generally the results seem to be better than in RANS simulations. It should be mentioned that no grid convergence was achieved similar to comparable LES investigations [13]; the authors [12] explained this as the result of '*running a complex numerical-physical system with numerous sources of error …; the reduction of one error does not drive the solution towards perfection*'. Finally, in two recent publications concerned with the DES approach, by Strelets [14] and Squires *et al.* [15], some new results predicted for more complex geometries, namely the flow around an airplane carriage and around a forebody cross-section, are presented. However, these are difficult to evaluate.

In spite of a wide range of DES applications which are available in the literature, in most of these investigations the results determined by the DES approach were compared with RANS simulations only. A detailed comparison with LES could also be very useful in order to see which of the advantages of LES could be reached in the framework of DES. Furthermore, it is worthwhile to determine more sharply its main disadvantages, as a price for the lower computational resources required. A direct comparison would be favourable if both DES and LES simulations would be carried out based on the same code and, probably, using the same spatial and temporal discretization. This procedure guarantees that numerical and implementation issues play no role in the comparison of the results. Therefore, the evaluation can be restricted to the modelling aspects. Of special importance in this context is how the modified S–A model performs as a subgrid model in the LES mode of the DES prediction. Of course, such an investigation is still not possible for very high Reynolds numbers. Therefore, a small *Re* was chosen for the present study, which allows the application of LES. The goal of the work was an attempt to locate some error sources of the DES technique and to compare and evaluate all three kinds of simulation techniques (DES, LES and RANS) for the

same—or as similar as possible—conditions. The subject of the investigation, namely an inclined flat plate, has a very simple geometry and is a representative of high-lift aerodynamic flows with a massive separation region. This configuration was chosen as a preliminary test case for the flow past an airfoil at the same conditions. It has proven to be a good choice, since we found very similar flow features as well as comparable results for both cases [16, 17]. Furthermore, the flow configuration studied allows a detailed investigation especially of the LES mode of the DES predictions. Owing to the fixed separation at the sharp leading edge, the RANS region is restricted to a narrow gap near the wall. Hence the DES approach has to work nearly completely in the LES mode, which allows one to evaluate the performance of the S–A model as a subgrid scale model and additionally the coupling with the RANS region. Based on the results obtained, which include pressure and velocity distributions, total lift and drag coefficients, vortex shedding frequency, Reynolds stresses, unsteady vorticity, etc., the main advantages and disadvantages of the applied methods (DES, LES, RANS) are compared with each other.

The paper is organized as follows. First, the governing equations are given for the LES and the RANS simulations. Second, in Section 3, the modelling approaches are described in detail for DES and RANS, whereas this issue is only briefly addressed for LES. Section 4 gives an overview of the numerical solution method applied. In the subsequent section the geometry and the details of the flow configuration are defined, including details on the grids and boundary conditions used. Finally, in Section 6, the results are presented and analysed, leading to an improved DES formulation.

2. GOVERNING EQUATIONS

An incompressible fluid with constant fluid properties is considered. The governing equations are the Navier–Stokes equations describing the conservation of mass and momentum. In the case of LES, these equations are filtered in space with the filter width Δ in order to separate large- and small-scale motions, which leads to the so-called filtered Navier–Stokes equations. In the RANS approach, the same equations are time averaged (or ensemble averaged), leading to the well-known RANS equations. Both kinds of equations can be written in a common (dimensionless) form:

$$\frac{\partial \bar{u}_j}{\partial x_j} = 0 \tag{1}$$

$$\frac{\partial \bar{u}_i}{\partial t} + \frac{\partial (\bar{u}_i \bar{u}_j)}{\partial x_j} = -\frac{\partial \bar{p}}{\partial x_i} - \frac{1}{Re}\frac{\partial \tau_{ij}^{\mathrm{mol}}}{\partial x_j} - \frac{\partial \tau_{ij}^{\mathrm{turb}}}{\partial x_j} \tag{2}$$

$$\tau_{ij}^{\mathrm{mol}} = -2\nu \bar{S}_{ij} \quad \text{where } \bar{S}_{ij} = \frac{1}{2}\left(\frac{\partial \bar{u}_i}{\partial x_j} + \frac{\partial \bar{u}_j}{\partial x_i}\right) \tag{3}$$

where u_i, p and $\nu = \mu$ ($\rho = 1$) are the velocity component, the pressure and the viscosity, respectively. In LES the overbar ($\bar{\cdot}$) defines the resolved scales, whereas in RANS it denotes the time-averaged components. Re is the characteristic Reynolds number defined below. The term τ_{ij}^{mol} describes the momentum transport due to molecular motion, which for a Newtonian fluid is given by Equation (3). Owing to filtering (LES) or time-averaging (RANS) of the

non-linear convective term in the momentum equation (2), the additional term τ_{ij}^{turb} arises which has to mimic the momentum transport due to turbulence motion. In the case of LES, τ_{ij}^{turb} is denoted as the subgrid scale (SGS) stress tensor and restricted to the influence of the non-resolved small-scale structures on the resolved large eddies. However, in RANS τ_{ij}^{turb} signifies the Reynolds stress tensor describing the influence of the entire spectrum of all length scales on the averaged flow field. In both cases this unknown has to be modelled. The modelling approaches are described in detail for DES and RANS in the next section. For LES only a brief description is given. More details on this topic can be found elsewhere [18, 19].

3. MODELLING APPROACHES

3.1. DES and RANS

As already mentioned above, the DES approach is based on a non-explicit splitting of the computational domain into two zones. In the first region near solid walls, the conventional RANS equations have to be solved. Within the second region, the governing equations are the filtered Navier–Stokes equations of the LES approach. In principle, the DES concept allows one to apply totally different models for the two regions, which would be a natural choice since the models have clearly distinguishable tasks. However, following the concept of Spalart *et al.* [1, 2, 7, 12], in both cases the S–A turbulence model [9] is used either as a *normal* turbulence model or as an SGS model, respectively. The model and the mechanism, which allows it to be applied in both the RANS and LES modes are described briefly.

The S–A model is based on Boussinesq's approximation, which describes the stress tensor τ_{ij}^{turb} as the product of the strain rate tensor $\bar{S}_{ij}$ (see Equation (3)) and an eddy viscosity ν_T:

$$\tau_{ij}^{\text{turb},a} = \tau_{ij}^{\text{turb}} - \delta_{ij}\tau_{kk}^{\text{turb}}/3 = -2\nu_T\bar{S}_{ij} \tag{4}$$

where $\tau_{ij}^{\text{turb},a}$ is the anisotropic (traceless) part of the stress tensor τ_{ij}^{turb} and δ_{ij} is the Kronecker delta. The trace of the stress tensor is added to the pressure, resulting in the new pressure $P = \bar{p} + \tau_{kk}^{\text{turb}}/3$.

The determination of the eddy viscosity ν_T is based on the solution of an additional transport equation. It was derived by Spalart and Allmaras [9] by taking the empiricism and arguments of dimensional analysis, the Galilean invariance and the selective dependence of the molecular viscosity into account. The governing equation for the new eddy viscosity variable $\tilde{\nu}$ forming the one-equation S–A model (low-*Re* variant) is

$$\underbrace{\frac{\partial\tilde{\nu}}{\partial t}}_{\text{local change}} + \underbrace{u_i\frac{\partial\tilde{\nu}}{\partial x_i}}_{\text{convection}} = \underbrace{c_{b1}\tilde{S}_\nu\tilde{\nu}}_{\text{production}} + \underbrace{\frac{1}{\sigma}\{\nabla\cdot[(\nu+\tilde{\nu})\nabla\tilde{\nu}] + c_{b2}(\nabla\tilde{\nu})^2\}}_{\text{diffusion}} - \underbrace{c_{w1}f_w\left[\frac{\tilde{\nu}}{d}\right]^2}_{\text{destruction}} \tag{5}$$

The left-hand side of Equation (5) represents local and convective changes of the transport variable $\tilde{\nu}$; the right-hand side includes the production term, the diffusion term and finally the destruction term for the reduction of the stresses in the vicinity of solid walls. It represents the dissipation of the turbulent kinetic energy in the near-wall region. Owing to its physical nature, in the RANS mode the destruction term is directly related to the reciprocal of the minimal wall distance d. Consequently, the boundary condition for the intermediate variable $\tilde{\nu}$ at solid

walls is $\tilde{\nu}=0$. The production term includes the scalar quantity $\tilde{S}_\nu$ which is expressed by the quantity S_ν plus a near-wall correction (see Equation (6)). The term S_ν can be modelled differently (e.g. by $|S_{ij}|$); however, as in the original model [9], S_ν is chosen here as the magnitude of the vorticity $|\boldsymbol{\omega}|$. The derivation of the missing relations

$$\nu_T=\tilde{\nu}f_{v1},\quad \tilde{S}_\nu\equiv S_\nu+\frac{\tilde{\nu}}{\kappa^2 d^2}f_{v2},\quad S_\nu=|\boldsymbol{\omega}|,\quad \chi\equiv\frac{\tilde{\nu}}{\nu} \tag{6}$$

$$f_{v1}=\frac{\chi^3}{\chi^3+c_{v1}^3},\quad f_{v2}=1-\frac{\chi}{1+\chi f_{v1}},\quad f_w=g\left[\frac{1+c_{w3}^6}{g^6+c_{w3}^6}\right]^{1/6} \tag{7}$$

$$g=r+c_{w2}(r^6-r),\quad r\equiv\frac{\tilde{\nu}}{\tilde{S}_\nu\kappa^2 d^2} \tag{8}$$

can be found in Reference [9]. The corresponding constants are $\kappa=0.41$, $\sigma=2/3$, $c_{b1}=0.1355$, $c_{b2}=0.622$, $c_{v1}=7.1$, $c_{w1}=c_{b1}/\kappa^2+(1+c_{b2})/\sigma$, $c_{w2}=0.3$ and $c_{w3}=2$.

This is the standard RANS formulation of the S–A model. The modification of this model for the DES approach is based on the following idea [1, 2, 7, 12]. Under the condition of local equilibrium, the production term ($\sim\tilde{S}_\nu\tilde{\nu}$) in Equation (5) is balanced by the destruction term ($\sim(\tilde{\nu}/d)^2$). This local balance leads to the relation $\tilde{\nu}\sim\tilde{S}_\nu d^2$, which is very similar to the relation given by the Smagorinsky subgrid scale model [8] used for LES (see Section 3.2) if the wall distance d is replaced by the filter width Δ. This analogy allows one in principle to apply the S–A model as a subgrid scale model if the wall distance d in Equations (5), (6) and (8) is substituted by a characteristic length scale proportional to Δ. Replacing d by the new variable $\tilde{d}$

$$\tilde{d}\equiv\min(d, C_{\mathrm{DES}}\cdot\Delta)\quad\text{with}\quad \Delta\equiv\max(\Delta x,\Delta y,\Delta z) \tag{9}$$

leads to a uniform model for the RANS and the LES mode of the DES approach. The recommended value for the adjustable parameter on structured grids is $C_{\mathrm{DES}}=0.65$. If the grid is fine enough to resolve vortex structures far away from the wall or within separated flow regions and is almost isotropic such as for a conventional LES, the relation $d>\Delta$ will guarantee that Equation (5) is used as an SGS model. Otherwise, because of the extremely fine grids required for LES computations of the near-wall flow (especially at high Re), it is not desirable to use this technique in this specific region. Therefore, the RANS approach should be applied for $d<\Delta$ and $\tilde{d}$ should be defined in the original manner ($\tilde{d}=d$). Within thin boundary layers near walls, the RANS approach also requires fine grids. However, in contrast to LES, for RANS a fine resolution of the wall normal direction (e.g. Δy) is often sufficient. This leads to highly stretched grids in the vicinity of walls, where only the Δy values are small in comparison with the wall distance d, and Δx and/or Δz are much larger. Thus, it should be mentioned that the definition of the filter size Δ in the LES mode [Equation (9)] differs from that of conventional subgrid scale models, which typically scale the filter width with the size of the control volume, i.e. $\Delta=(\Delta x\cdot\Delta y\cdot\Delta z)^{1/3}$. However, relation (9) guarantees the desired behaviour of the model including the switch-over between the two modes (RANS/LES). The region corresponding to $d\sim\Delta$ is called *grey area* by the authors of DES [1, 2, 7, 12]. This notation is chosen because it is not clear what exactly happens in this region and how significant the role of modelled and resolved vortical structures existing between the RANS and LES zones is. The non-explicit character of the splitting of the flow

zones means that a predefined distribution of grid cells can be used for an implicit definition of an RANS region. For example, for two similar grids with only different resolutions in the spanwise direction, the RANS regions will not be the same.

Concerning the resolved vortical structures, the following should be mentioned. Unlike in LES, not only will the small-scale eddies smaller than the grid cells be filtered out, but also the eddies scaled with the grid cells in a boundary layer will not be resolved, because they are in the region which is modelled by RANS. Owing to this, it is assumed that the DES approach should be most effective for flows consisting of regions with thin attached boundary layers (I) and separated regions which are controlled by large, unsteady vortical structures (II). Flow regions of type (I) can be predicted reliably and efficiently by the RANS approach, whereas LES is also appropriate but extremely expensive. On the other hand, flow phenomena of type (II) cannot be computed reliably by RANS. For this purpose, LES is the superior tool. Furthermore, such flows with attached and separated regions are the most natural choice for DES in order to guarantee the coupling of the RANS and the LES region in the *grey area*. In conclusion, the DES concept is expected to work most efficiently for this special class of flows. The main expectations are:

- saving computational resources compared with pure LES and
- predicting separated flows more reliably than pure RANS.

3.2. LES

In principle, the LES concept leads to a closure problem similar to that obtained by the RANS approach. Therefore, a similar classification of turbulence models starting with zero-equation models and ending up with full stress models is possible. However, the non-resolvable small scale in an LES is much less problem dependent than the large-scale turbulence so that the subgrid scale turbulence can be represented by relatively simple models, e.g. zero-equation eddy-viscosity models. Like the S–A model for DES and RANS, the well known and most often used Smagorinsky model [8] is based on Boussinesq's approximation given by Equation (4). The eddy viscosity ν_T itself is a function of the strain rate tensor $\bar{S}_{ij}$ and the subgrid length l:

$$\nu_T = l^2 \,|\bar{S}_{ij}| \quad \text{with } l = C_s \Delta \left[1 - \exp\left(\frac{-y^+}{A^+}\right)^3\right]^{0.5}$$

$$\Delta = (\Delta x \cdot \Delta y \cdot \Delta z)^{1/3}, \quad y^+ = \frac{y u_\tau}{\nu}, \quad u_\tau = \sqrt{\frac{\tau_w}{\rho}} \quad \text{and} \quad A^+ = 25 \tag{10}$$

C_s is the well-known Smagorinsky constant, which has to be prescribed as a fixed value in the entire integration domain or can be determined as a function of time and space by the dynamic procedure originally proposed by Germano *et al.* [20] and later improved by several authors, e.g. Reference [21]. In the first case, a Van Driest damping function is required [see Equation (10)] in order to take the reduction of the subgrid length l near solid walls into account. In the present investigation, the fixed parameter version of the Smagorinsky model with a standard constant $C_s = 0.1$ was applied. Even though it is well known that the dynamic model is superior for free shear layer flows, it is not considered in this study. The reason

for that lies in the SGS type of model within the LES mode of the DES formulation. The way the modified S–A model is used as an SGS model in the LES mode strongly resembles the Smagorinsky model with a corresponding constant C_{DES}. Further investigations could deal with a comparison of both methods using a dynamic type of model for either the Smagorinsky model in LES and the S–A model in DES. Additionally, the influence of the SGS model is expected to be small owing to the low Reynolds number of this investigation as this was the case for similar configurations (see, e.g. Reference [19]).

4. NUMERICAL METHODOLOGY

The same computer code $\mathcal{LESOCC}$ [18, 19] is used for all three approaches to reduce the influence on the final results of different spatial and time discretizations, various solvers for the system of linear equations and other numerical and implementation details. The code is based on a 3D finite-volume method for arbitrary non-orthogonal and block-structured grids. All viscous fluxes are approximated by central differences of second-order accuracy, which fits the elliptic nature of the viscous effects. As shown in Reference [19] and by other authors, e.g. [22], the quality of LES predictions is strongly dependent on low-diffusive discretization schemes for the non-linear convective fluxes in the momentum equation (2). Although several schemes are implemented in the code applied, the central scheme of second-order accuracy (CDS-2) is preferred for the LES and the DES predictions in the present work. In the pure RANS case, this issue is much less critical than for the other approaches. Therefore, in addition to the CDS-2 scheme, the HLPA scheme (Hybrid linear/parabolic approximation) proposed by Zhu [23] was used. It combines a second-order upstream-weighted approximation with first-order upwind differencing under the control of a convection boundedness criterion. The main advantage of this scheme for the RANS case is that it leads to faster convergence towards a steady state compared with CDS-2. Furthermore, any numerical oscillations that might occur in predictions based on CDS-2 if the local value of the Peclet number $Pe=u\Delta x/v$ is >2 are suppressed by the HLPA scheme. However, as was proved in the present study, the difference in the RANS results when using CDS-2 and HLPA are only marginal. Therefore, this specific feature of the RANS predictions does not influence the final results.

Time advancement is performed by a predictor–corrector scheme. A low-storage multi-stage Runge–Kutta method (three sub-steps, second-order accuracy) is applied for integrating the momentum equations in the predictor step. Within the corrector step the Poisson equation for the pressure correction is solved implicitly by the incomplete LU decomposition method of Stone [24]. Explicit time marching works well for LES/DES with small time steps which are necessary to resolve turbulence motion in time. For the RANS predictions an implicit method might be more efficient, but this was not the topic of the present investigation. The pressure and velocity fields on a non-staggered grid are coupled by the momentum interpolation technique of Rhie and Chow [25] which is uncritical for LES if design rules for appropriate grids are taken into account [26]. The S–A model for the RANS and DES computations requires the solution of the additional scalar transport equation (5), which is discretized in the same way as the momentum equations (2). The code is highly vectorized and additionally parallelized by domain decomposition with explicit message passing based on MPI, allowing efficient computations especially on vector-parallel machines and SMP clusters. The simulations were partially carried out on a Fujitsu VPP 300/700 applying four processors and partially on a

Hitachi SR 8000-F1 applying eight nodes (8×8 processors). A variety of different test cases (see, e.g. References [13,16–19]) served for the purpose of code validation.

5. DESCRIPTION OF THE CONFIGURATION

The geometric configuration of the flow around an inclined flat plate mounted inside a plane channel is shown schematically in Figure 1. The entire flow domain extends to approximately six times the plate length c in main flow direction. The height of the channel is $3c$. As shown in a previous investigation by the authors [16], the spanwise extension of the computational domain is of great importance for reliable LES predictions of this flow. Therefore, a spanwise extension of one plate length c, which was earlier found to be sufficient [16], was chosen for the present study. The flat plate is placed exactly in the vertical middle of the channel and inclined at an angle of $\alpha=18°$. This configuration is chosen according to the COSTWING experiment initiated by Lerche and Dallmann [27], which aims at the flow around an airfoil at high angles of attack. Instead of a flat plate, a nominally 2D airfoil based on an NACA-4415 profile is mounted inside a wind and a water tunnel. The Reynolds number based on the chord length c and the free-stream velocity u_∞ can be varied in the range $8\times10^4\leqslant Re_c\leqslant8\times10^5$ and the angle of attack in the range $0°\leqslant\alpha\leqslant22.5°$. The main purpose of COSTWING is a detailed study of the physics of separated turbulent flows, including the detection of coherent structures. Furthermore, the experimental results not yet available should serve as a database for the validation of different numerical simulations. Here it is used as a basic principle by adapting the configuration to a more simplified case, alleviating the numerical effort and fixing the separation to the sharp leading edge. The inclination of $\alpha=18°$ was selected exemplarily because detailed LES investigations used for the purpose of comparison are already available [16].

In consideration of a reasonable resolution for the numerical simulation of the flow around the inclined flat plate, a Reynolds number $Re_c=20\,000$ was chosen. At this Reynolds number no-slip boundary conditions ($u=v=0$) can be applied at the surface of the plate. In order to avoid extensive computational costs, the boundary layers of the channel walls are not resolved, but slip conditions ($\partial u/\partial y=v=\partial w/\partial y=0$) are utilized instead. Owing to the

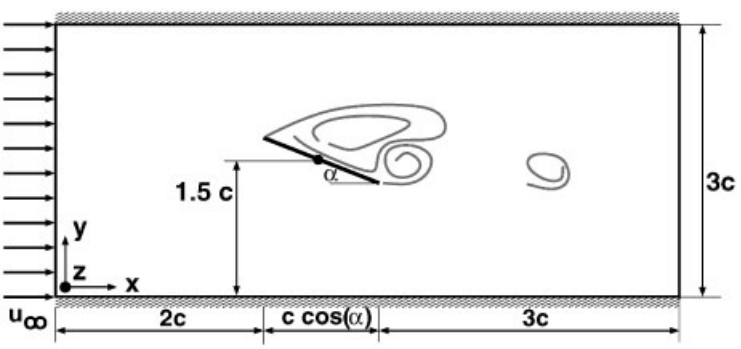

Figure 1. Sketch of the flow configuration considered.

Table I. Grid information for the simulations performed; all geometrical quantities are non-dimensionalized by the chord length c.

Case	Total No. of CVs	CVs along one plate side	CVs in spanwise direction	CVs in B.L. for non-inclined plate	Wall normal and tangent grid spacing
RANS-C	2.76×10^4	92	2D	17	0.001
RANS-F	5.20×10^4	128	2D	20	0.001
DES-C	0.99×10^6	92	36	17	0.001
DES-F	1.87×10^6	128	36	20	0.001
LES-C	0.99×10^6	92	36	17	0.001
LES-VF	8.97×10^6	298	76	23	0.001

experimental set-up, either statistically two-dimensional or spanwise periodic structures can be expected. Therefore, in the present numerical simulations, periodicity in the spanwise direction is assumed as in References [16, 17], applying a sufficiently large spanwise domain size of $z_{\max}=1\times c$. A constant velocity u_∞ without any perturbations is prescribed at the inlet two plate lengths in front of the plate assuming a laminar oncoming flow. At the outlet, a convective boundary condition given by

$$\frac{\partial u_i}{\partial t}+u_{\text{conv}}\frac{\partial u_i}{\partial x}=0 \tag{11}$$

ensures that vortices can pass through the outflow boundary without any significant disturbances for the internal integration domain. Here, u_{conv} is set to u_∞.

As explained above, different simulation approaches (RANS, DES, LES) with different grid resolutions were employed to simulate the flow configuration described. Some detailed grid information about the particular cases is provided in Table I. The grid points are clustered in the vicinity of the infinitely thin plate and towards the leading and trailing edges (see Figure 2). All simulations have the same grid spacing in the first layer normal to the wall and in a tangential direction at the leading and trailing edges in common. In order to provide the possibility of comparing the resolution of the numerical grids, the number of control volumes lying inside the boundary layer for a non-inclined plate flow at the same Reynolds number is also listed in Table I. Using an identical coarse grid of about one million control volumes, both a DES (DES-C) and an LES (LES-C) prediction were performed, thus allowing a direct comparison of these two methods, the grid influence being eliminated. A DES on a somewhat finer grid (DES-F) with about two million CVs and an LES on a very fine grid (LES-VF) consisting of about 9 million CVs were also carried out. The latter should be used to evaluate the other simulations as being the most accurate in terms of resolution. Additionally, two- and three-dimensional RANS simulations (RANS-C, RANS-F) were performed. However, the three-dimensional predictions yield no three-dimensional structures in the wake of the inclined plate. Hence the results of 2D- and 3D-RANS are identical in an x–y cross-section. Therefore, in Table I only the two-dimensional cases whose grids are based on a cross-section of the corresponding three-dimensional grid are included. Taking all cases in Table I into account, the three different simulation techniques can be compared with each other, based on the same

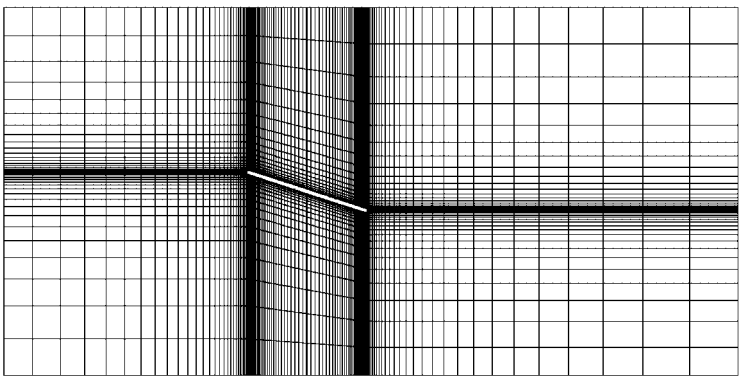

Figure 2. x–y plane of the computational grid for LES-VF simulation. Only every fifth grid line is shown.

resolution. Additionally, the influence of the grid resolution can be studied for each method separately.

In the DES calculations the parameter C_{DES} is set to the recommended value of $C_{\mathrm{DES}} = 0.65$. Considering the grid distance in the spanwise direction as being the largest (36 CVs in a spanwise domain size of c), this leads to switching between RANS and LES in a distance $0.02\,c$ away from the wall. Consequently, the RANS region is restricted to a very narrow zone in the vicinity of the wall, whereas the entire remainder of the computational domain is computed in the LES mode. The present configuration especially allows one to evaluate the performance of the modified S–A model working as a subgrid scale model.

6. RESULTS AND DISCUSSION

The main characteristics of the instantaneous and time-averaged flow around the inclined plate are known from a previous study purely based on LES [16]:

- The flow field around the inclined plate under the conditions investigated ($Re_c = 20\,000$ and $\alpha = 18°$) is controlled by an asymmetric vortex shedding cycle with a Strouhal number $St' = fc'/u_\infty \approx 0.2$ scaled with the windward width $c' = c \sin \alpha$.
- The flow at the plate and in the wake is strongly dominated by the development and shedding behaviour of the trailing-edge vortex. This strong vortex structure develops almost periodically in the vicinity of the trailing edge.
- At the leeward side of the plate a large clockwise rotating recirculation region of nearly constant pressure exists which originates from the separation at the sharp leading edge. In the separated shear layer where transition takes place, a Kelvin–Helmholtz instability is observed.
- The life cycle of the trailing-edge vortex also determines the structure and size of this recirculation region on top of the plate.

These observations based on LES predictions were found to be in close agreement with the experimental findings of different authors, e.g. Reference [28] and references therein,

[29, 30]. The objectives of the present investigation were to prove the applicability of DES (and RANS) for this flow and to compare the quality of the predicted results for all three approaches (RANS, DES and LES) with each other. The LES calculation on the finest grid (LES-VF, see Table I) will serve as a reference case.

Some remarks on the calculations are required prior to the analysis. Although RANS predictions on different grids were carried out, in the following only the case of the fine grid (RANS-F) is considered and discussed in detail. Because the differences between the results on both grids were marginal, the RANS prediction on the fine grid is grid independent and it is therefore not necessary to discuss results obtained with different resolutions. Furthermore, it is important to mention that all computations based on RANS, although applied in an unsteady mode known as URANS, do not show the unsteady shedding motion discussed above. Instead, the RANS simulations converge to steady-state results. Hence they are not capable of describing the unsteady nature of the flow field around the inclined plate. In contrast, the DES and LES predictions yield the main characteristics of the unsteady flow field. In order to compare all results including RANS, the DES and LES computations are averaged both in time and in space (spanwise). For all simulations performed an averaging in time of at least 50 dimensionless time units was made. The additional averaging in the spanwise direction is done in order to obtain a well-averaged flow field more rapidly and therefore to save computing time. The analysis will start with the averaged flow field (Section 6.1). In the second and third parts, also the unsteady flow field (Section 6.2) and the higher-order statistics (Section 6.3) of the DES and LES predictions are discussed. Finally, the results are analysed with respect to the performance of the SGS models applied in pure LES and the LES mode of the hybrid DES predictions (Section 6.4). Based on this analysis, some modifications of the S–A model are proposed for the use as an SGS model within the DES approach strongly enhancing the quality of the predictions.

6.1. Averaged flow field

In Figure 3, the averaged flow field of all simulations is shown by streamlines. The oncoming flow separates at the leading edge and forms a large recirculation region rotating in clockwise (cw) direction on the leeward side of the plate. A second vortex originates at the trailing edge due to the roll-up of the shear layer there. This vortex is rotating counterclockwise (ccw) and is smaller in size. All simulations performed are capable of predicting these overall flow features, but at a closer look there are significant deviations between them. One difference appears in the location of the recirculation region and the trailing-edge vortex. Table II provides the co-ordinates of the centres for both the cw and ccw rotating vortices. In the vertical direction (y/c), these centres are fairly well aligned, but there are considerable deviations in the horizontal position (x/c) between some of the simulations. This holds especially for the RANS-F result for which a horizontal displacement of the clockwise rotating vortex of about $0.21c$ with respect to the LES-VF calculation can be observed. That represents an error of 22.5%. The DES results on the coarse grid (DES-C) exhibit, for the same clockwise rotating vortex, an offset of $\approx 0.07c$, whereas the centre position of this vortex provided by the DES-F and LES-C simulations nearly coincide with that of the LES-VF. Both LES calculations indicate almost the same centre position for the trailing-edge vortex. All other simulations show in equal measure a small deviation therefrom, where the largest deviations in the x-direction ($\approx 7.5\%$) are again found for the RANS-F case. As can be seen in Figure 3, this

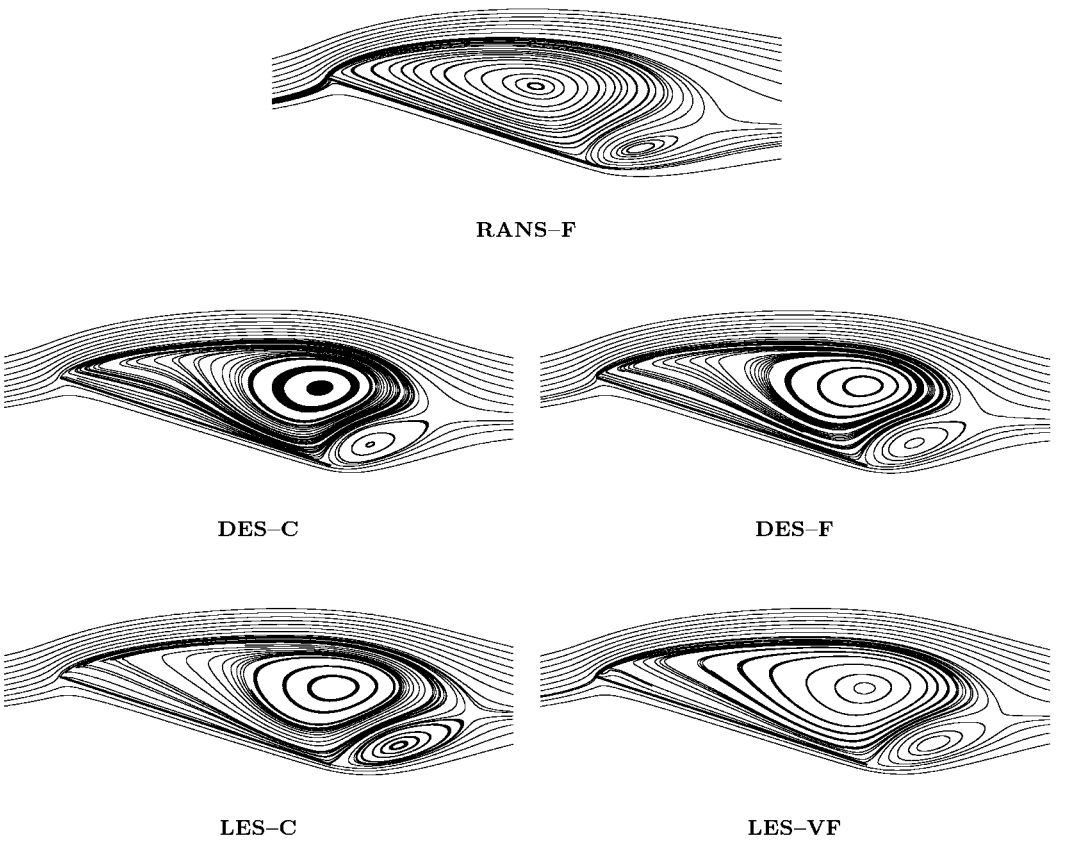

Figure 3. Streamlines of the averaged flow field for the five different simulations defined in Table I. $Re_c = 20\,000$ and $\alpha = 18^\circ$.

observation corresponds to different locations of the trailing-edge vortex. In the RANS and both DES predictions this flow structure partially resides upon the end of the plate, whereas in both LES computations this vortex is shifted completely behind the plate.

Figure 4 depicts the pressure contours of the averaged flow field for all simulations performed. For better comparability of the different cases, the reference point of the pressure is adjusted in such a way that a dimensionless stagnation point pressure of $\bar{p} = 1$ is reached. In all three-dimensional simulations both for DES and LES, the pressure minimum is located near the centre of the trailing-edge vortex given in Table II. The pressure contours of both DES cases look similar to both LES cases except in the region of the free shear layer near the leading edge of the plate. In contrast, the RANS-F case exhibits a strongly deviating contour plot, where the pressure minimum lies behind the leading edge of the plate. The quantitative value of the negative pressure peak varies over a wide range among all simulations, as can be seen from the contour plot legends.

These quantitative differences between the simulation results are also visible in the C_p distribution along the plate surface (see Figure 5). All cases predict a nearly constant pressure

Table II. Location of the centre of vortices. The origin is set to the leading edge of the plate.

	cw rotating vortex			ccw rotating vortex		
Case	x/c	y/c	Symbol	x/c	y/c	Symbol
RANS-F	0.733	−0.026	●	1.097	−0.247	○
DES-C	0.878	−0.041	▲	1.108	−0.228	△
DES-F	0.945	−0.028	▼	1.120	−0.231	▽
LES-C	0.965	−0.038	◆	1.194	−0.243	◇
LES-VF	0.946	−0.040	■	1.186	−0.236	□

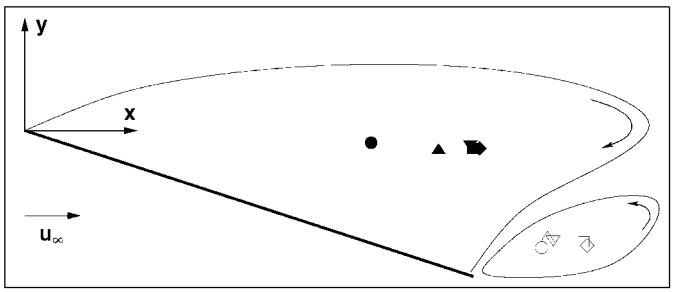

on the upper side in the large recirculation region, as expected in stalled configurations such as this. However, the level of this constant pressure is unequal. The deviations with respect to the reference simulation (LES-VF) are largest for RANS-F, followed by DES-C and DES-F. The LES on the coarse grid (LES-C) overpredicts the pressure on the suction side of the plate only slightly. Since the flow remains attached on the lower side, the differences between the different approaches are smaller except for the RANS-F case. However, owing to different conditions at the trailing edge of the plate, the deviations between the various simulations at the leeward side are increasing towards the edge. The differences in the pressure distribution on the two sides finally lead to varying lift and drag forces, which will be considered in the next section.

A more thorough comparison of the conducted simulations with respect to quantitative results can be accomplished by looking at the velocity profiles shown in Figure 6. The tangential velocities of the averaged flow field are displayed at three different locations above the plate ($x/c=0.2$, 0.6 and 1.0) and two locations in the wake ($x/c=1.2$ and 1.4) adjusted to an imaginary elongation of the plate. As indicated by the velocity profile of the reference simulation (LES-VF), back-flow occurs in the separated region along the entire plate surface. This trend is captured generally by all cases at the first and second locations depicted in Figure 6. However, at $x/c=1.0$ (trailing edge), only the coarse LES (LES-C) is in close agreement with the reference profile. The RANS and the DES calculations predict a positive tangential velocity there and deviate strongly from the LES simulations. This coincides with the observation of the different locations of the trailing-edge vortex mentioned above. Furthermore, the RANS-F results are not satisfactory over the entire plate. The absolute value of the velocity near the plate surface is overpredicted, which leads to a totally different profile shape. This is also true

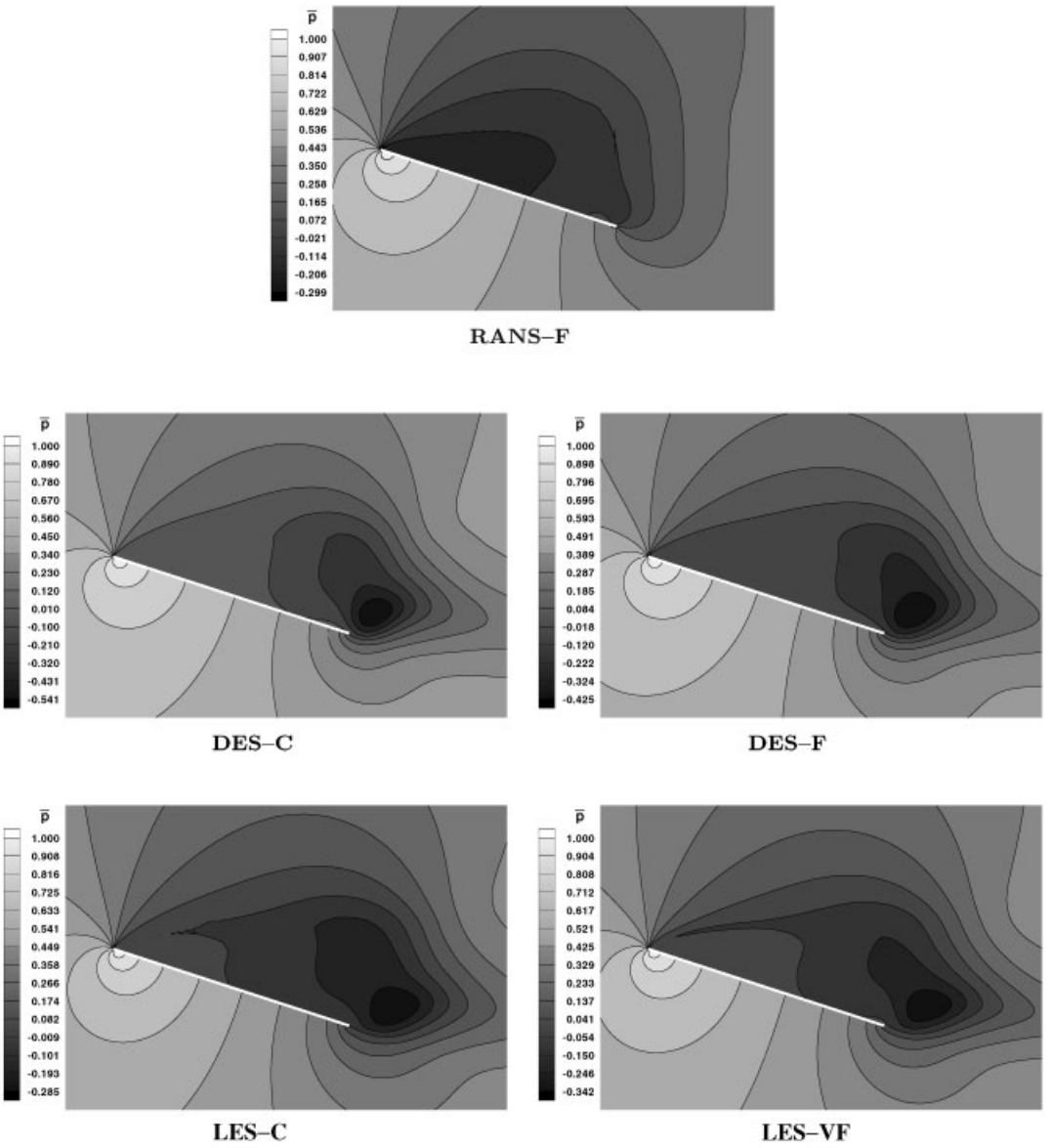

Figure 4. Pressure contours of the averaged flow field for the five different simulations defined in Table I. $Re_c = 20\,000$ and $\alpha = 18°$.

in the wake, where the RANS profile is much flatter than the others owing to overpredicted eddy viscosity values (see Section 6.4). Again, only the LES-C profile coincides with the reference data in the wake, whereas both DES cases are in agreement with respect to the shape of the profile, but not in the quantitative sense. These results confirm the inapplicability of the RANS approach for flows with large regions of separation and point to some deficiencies of the present DES approach.

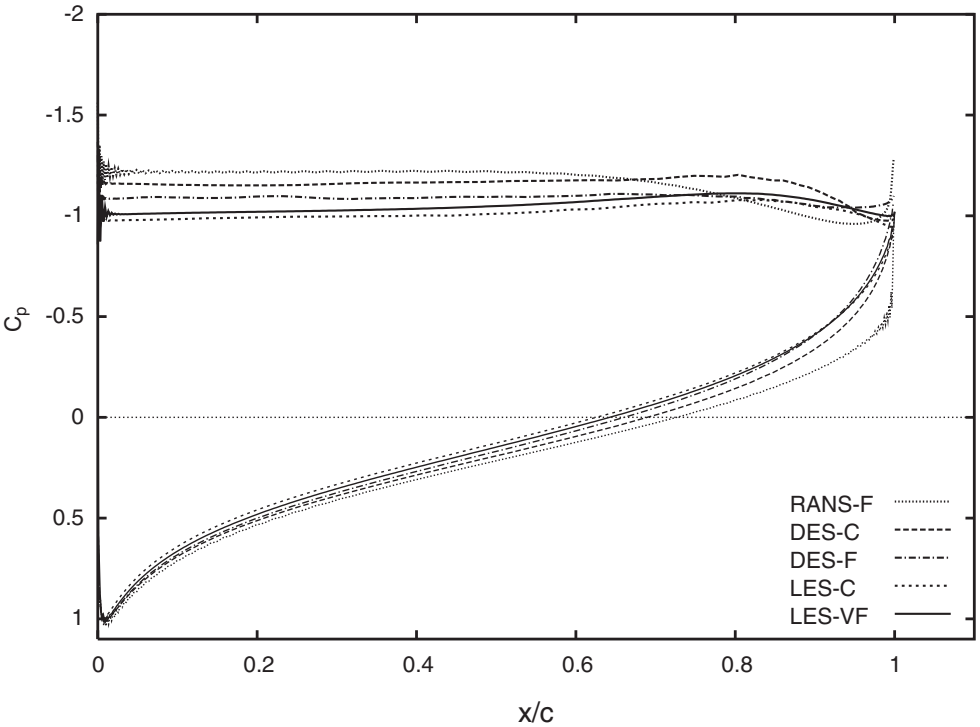

Figure 5. C_p distribution of the averaged flow field for the five different simulations defined in Table I. $Re = 20\,000$ and $\alpha = 18^\circ$.

6.2. *Unsteady flow field*

As known from a previous LES study [16] and already stated at the beginning of this section, the unsteady flow in the present configuration is strongly dominated by the activity of the trailing-edge vortices. The development and shedding of these vortices are accompanied by a frequency which can be determined by a fast Fourier transformation of the lift signal. Based on the plate length c (or the windward width $c' = c \sin \alpha$) and the inflow velocity u_∞, the characteristic frequency of the vortex shedding sequence results in a corresponding Strouhal number St (or St'). The predicted values of St and St' for all simulations, capable of capturing the unsteadiness of the flow, are given in Table III. They show a fairly good agreement with the reference simulation LES-VF, yielding a Strouhal number $St' \approx 0.19$. The largest deviation of about 3.6% is visible for DES-C, whereas LES-C generates a slightly too high value. Based on these observations, it follows that an important contribution to the unsteady motion of the flow is sufficiently well reproduced by all simulations (DES/LES), even on the coarse grid. However, as already pointed out by Rodi *et al.* [31], the accurate prediction of the Strouhal number for bluff-body flows is not necessarily an appropriate measure for the quality of the entire simulation.

Therefore, Table III provides additional values for the mean lift ($\bar{C}_l$) and drag ($\bar{C}_d$) coefficients, together with the standard deviations (σ_{C_l}, σ_{C_d}) of the corresponding time signals. The

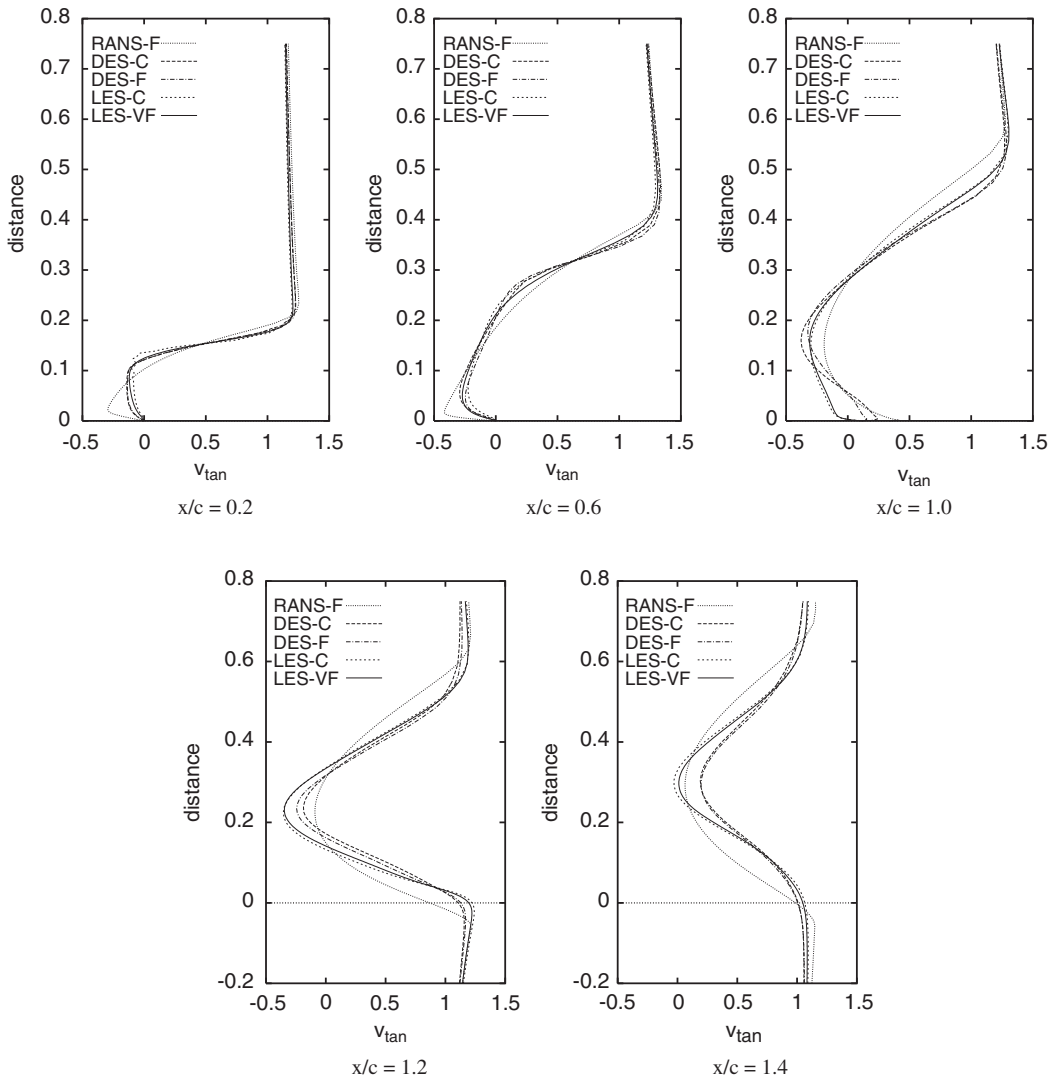

Figure 6. Profiles of the tangential velocities of the averaged flow field as a function of the wall-normal distance at five different locations (three on the plate, two in the wake). $Re_c = 20\,000$ and $\alpha = 18^\circ$.

small differences between the DES and LES cases with respect to the coefficients are within acceptable limits, demonstrating that both are capable of predicting these integral quantities in a satisfactory manner. Almost identical values for the standard deviations (σ_{C_l}, σ_{C_d}) are found, both of which are relatively small. These correspond to small amplitudes of the oscillating lift and drag signals, respectively. Comparing the two DES cases, it can be recognized that an improved grid resolution leads to a more accurate prediction of the lift and drag coefficients. The DES-F results are closer to the LES-VF case than the DES-C results. Comparing the DES-C and LES-C cases, which were performed using an identical grid, it is interesting to

Table III. Comparison of integral quantities for the flat plate at $Re_c = 20\,000$ and $\alpha = 18°$.

Case	$\bar{C}_l$	$\bar{C}_d$	σ_{C_l}	σ_{C_d}	St	St'
RANS-C	1.314	0.438	—	—	—	—
RANS-F	1.318	0.439	—	—	—	—
DES-C	1.182	0.399	$8.0 \cdot 10^{-2}$	$2.5 \cdot 10^{-2}$	0.60	0.185
DES-F	1.153	0.389	$8.1 \cdot 10^{-2}$	$2.5 \cdot 10^{-2}$	0.61	0.189
LES-C	1.078	0.365	$7.9 \cdot 10^{-2}$	$2.5 \cdot 10^{-2}$	0.63	0.195
LES-VF	1.128	0.380	$7.0 \cdot 10^{-2}$	$2.2 \cdot 10^{-2}$	0.62	0.192

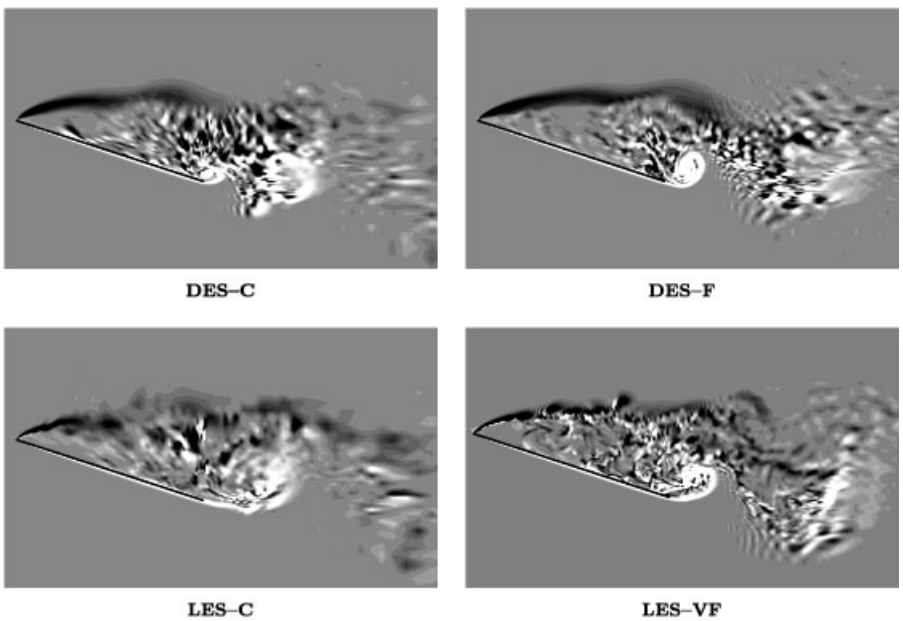

Figure 7. Contours of the vorticity component ω_z in an x–y plane, taken from the instantaneous flow field, for both DES and both LES predictions. $Re_c = 20\,000$ and $\alpha = 18°$.

see that both deviate in equal measure from the reference case. DES-C overestimates the coefficients to a similar extent by which LES-C deviates towards smaller values. In contrast to the small deviations between these predictions, the RANS computations result in far too large lift and drag coefficients. This tendency of the RANS approach towards a strong overprediction of the forces is already well known. It is also not surprising that applying RANS on a finer grid (RANS-F) does not improve the predicted values with respect to the coarse grid results (RANS-C).

Some of the differences between the DES and LES computations become understandable on looking at the contours of the vorticity component ω_z shown in Figure 7. The vorticity

is taken from the instantaneous flow field at an arbitrary time instant. The four parts of Figure 7 were not meant to represent a synchronous instant of the vortex shedding cycle, since this was not relevant for the purpose of showing them here. Anyhow, it seems that the snap shots of the DES-F and LES-VF vorticity contours do represent almost the same instant by chance. Compared with the LES on the very fine grid (LES-VF), the contours obtained by the other simulations are visibly smoother and do not show a large variety of resolved small-scale structures. This is particularly noticeable in the region of the leading-edge shear layer. In contrast, the LES-VF prediction reproduces this flow feature sharply, thus allowing the motion of single eddies in this region to be resolved in detail. Consequently, for the LES-VF case and at least allusively also for LES-C, it is possible to detect a Kelvin–Helmholtz instability occurring in the shear layer and leading to transition. Such detailed flow structures are not resolved by either DES calculation. Therefore, they fail to reflect the flow in this region properly. This will also become evident on looking at the higher-order statistics in the following section. Although the same grid is applied in the DES-C and the LES-C cases, the latter tends more clearly to the reference case. Hence the grid resolution is not solely responsible for the quality of the results. In contrast the modelling aspect plays the dominant role in this behaviour, which will be analysed in detail in Section 6.4.

6.3. Higher-order statistics

Higher-order statistics of the DES and LES simulations are shown in Figure 8 by contours of the turbulent kinetic energy $k = 1/2(\overline{u'u'} + \overline{v'v'} + \overline{w'w'})$. The components of the Reynolds stresses include the periodic and the turbulent fluctuations and are restricted to the resolved part. In order to separate periodic and turbulent components, phase averaging has to be carried out, which is associated with several difficulties owing to the slightly varying shedding periods, and was therefore omitted here. For all cases the largest values can be found in the vicinity of the trailing edge, mainly caused by the quasi-periodic shedding motion of the trailing-edge vortex. However, the shear layer originating at the leading edge of the plate is not equally well captured by the DES and the LES computations. In the LES-VF case a local maximum in the distribution of the turbulent kinetic energy is located somewhat downstream of the leading edge. It reflects the Kelvin–Helmholtz instability detected in the shear layer. This local maximum of k is not observed in the other three simulations depicted. Whereas the LES on the coarse grid (LES-C) tends to reproduce the shear layer similar to LES-VF, both DES computations are not capable of doing so and predict almost vanishing turbulent kinetic energy in the shear layer region. This large deviation between the DES and LES results coincides with the findings from the distribution of the unsteady vorticity component ω_z in the previous section, which already clearly demonstrated that the DES predictions are not able to resolve the Kelvin–Helmholtz instability in the free shear layer. Further discussion of this aspect will follow in more detail in the subsequent section.

Additionally, strong deviations exist for the maximum values of k found in the centre of the trailing-edge vortex. The DES overestimates the maxima of the resolved Reynolds stresses to a great extent, i.e. 39% for DES-C and 24% for DES-F according to the reference value from LES-VF. Thus a finer grid resolution (DES-F) improves the predicted values for DES, but they are still too large. In contrast for the LES on the coarser grid (LES-C), the resolved Reynolds stresses and k are underpredicted and therefore show the expected behaviour for a coarser resolution with respect to the fine resolution.

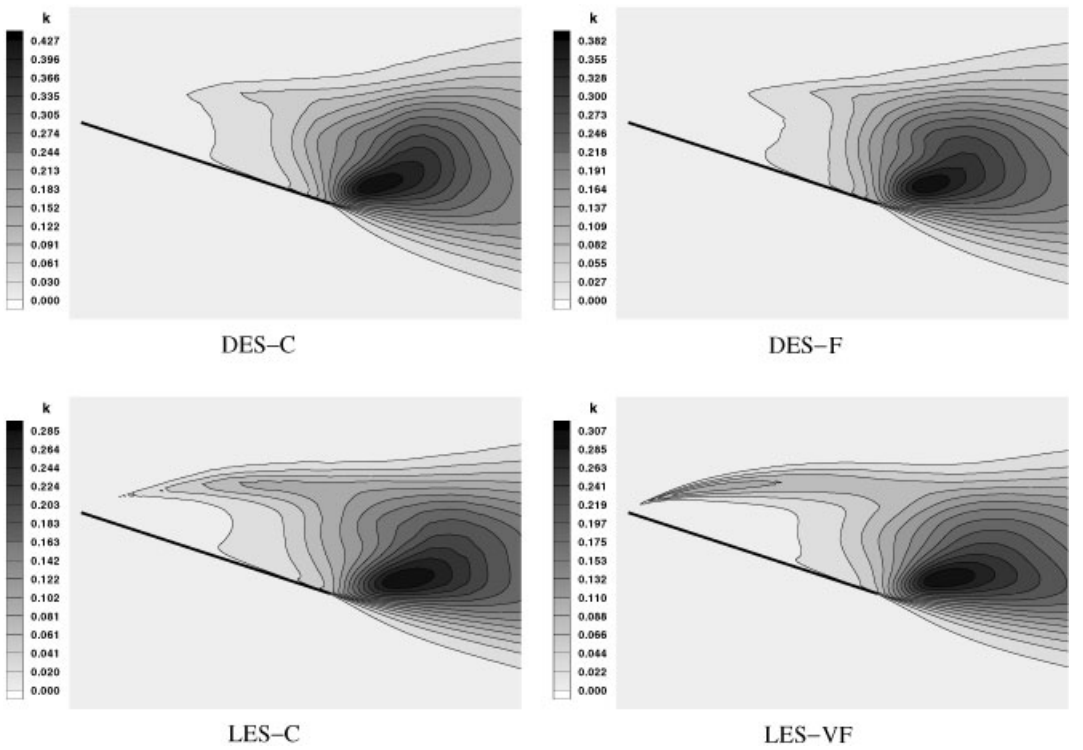

Figure 8. Resolved Reynolds stresses in terms of the turbulent kinetic energy $k = 1/2(\overline{u'u'} + \overline{v'v'} + \overline{w'w'})$ for the DES and LES cases. $Re_c = 20\,000$ and $\alpha = 18^\circ$.

Again, profiles of the different components provide a better insight into the quantitative differences between the various simulations. In Figures 9–11 the profiles of the Reynolds stress components $\overline{u'u'}$, $\overline{v'v'}$, and $\overline{u'v'}$ are depicted. For each component displayed, the LES-VF yields the largest absolute values at $x/c = 0.2$ in the form of a peak. This reflects the well-resolved shear layer originating from the leading edge. The DES simulations do not even come close to the LES-VF profile. Merely the LES-C profile seems to resemble that of the finer LES. At a more centred position on the plate ($x/c = 0.6$), a certain improvement can be observed, at least regarding the profile shapes. Particularly for the components $\overline{u'u'}$ and $\overline{u'v'}$ it can be stated that the profiles of all simulations look similar. Nevertheless, large quantitative discrepancies exist here, too. At the trailing edge of the plate the situation is worse again. As already realized in the contour plot legends of Figure 8, the DES calculations strongly overpredict the Reynolds stresses there. In addition the profile shapes of the DES and the LES results differ considerably. Close to the trailing edge, there is a local maximum in the $\overline{u'u'}$ and $\overline{u'v'}$ profiles of the DES cases. An equivalent feature does not exist in the LES profiles. Generally, the profile shapes of all simulations look rather similar in the wake, except perhaps for the $\overline{u'v'}$ profile at $x/c = 1.2$. However, quantitative discrepancies exist here also. As already noted for the mean velocity profiles, both LES cases are relatively close to each other with respect to all higher-order statistics whereas the DES prediction leads to much larger deviations. By the use of a finer grid, the DES-F results show a tendency towards the

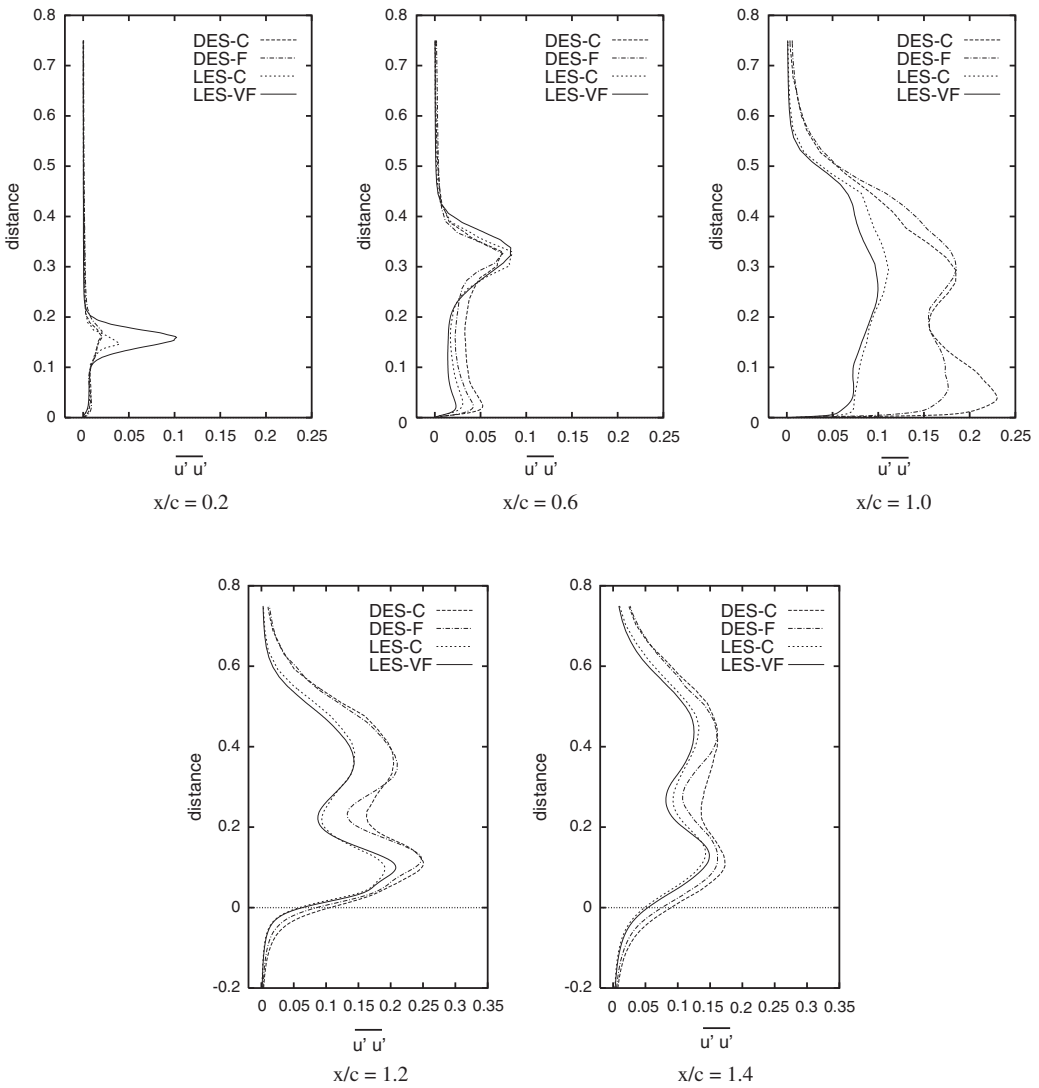

Figure 9. Profiles of the resolved Reynolds stress component $\overline{u'u'}$ as a function of the wall-normal distance at five different locations (three on the plate, two in the wake). $Re_c = 20\,000$ and $\alpha = 18^\circ$.

LES-VF profiles, but the agreement with the reference data is still much worse than for the coarse LES (LES-C). A direct comparison of the DES and LES results obtained on the same grid (DES-C, LES-C) clearly shows that the modelling aspect and not the resolution is the main cause of these findings.

6.4. Analysis of the differences between RANS, DES and LES

Very interesting differences are found in the distribution of the eddy viscosity with respect to the molecular viscosity shown in Figure 12. Starting with the LES-VF case, increased values

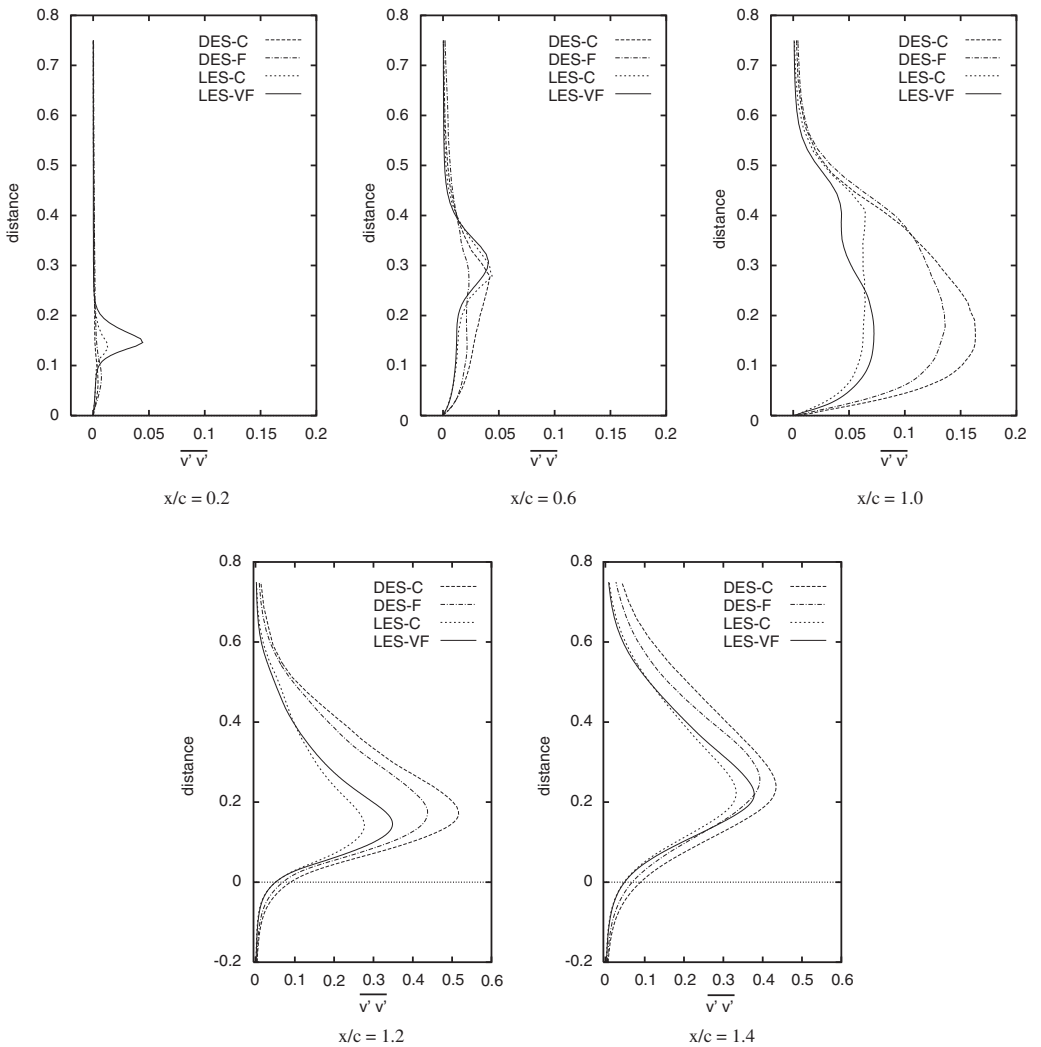

Figure 10. Profiles of the resolved Reynolds stress component $\overline{v'v'}$ as a function of the wall-normal distance at five different locations. $Re_c = 20\,000$ and $\alpha = 18°$.

of ν_T/ν can be observed in the shear layers and in regions of large vortical structures in the wake. The shear layer originating from the leading edge is reproduced in a particularly detailed fashion, including an accurate description of the eddy motion and the resolution of the Kelvin–Helmholtz instability in this region. In comparison with LES-VF ($\nu_T/\nu|_{\max} \approx 2$), the LES on the coarser grid (LES-C) yields as expected higher values of $\nu_T/\nu|_{\max} \approx 6$. This is natural, since on a coarser grid the filter size is larger and hence the eddy viscosity inherits a greater part in describing the turbulent motion. At the same time, the shear layer appears to be more spread, preventing a distinct reproduction of vortical motion. Thus, detailed information on the role of vortices occurring in the Kelvin–Helmholtz instability cannot be captured

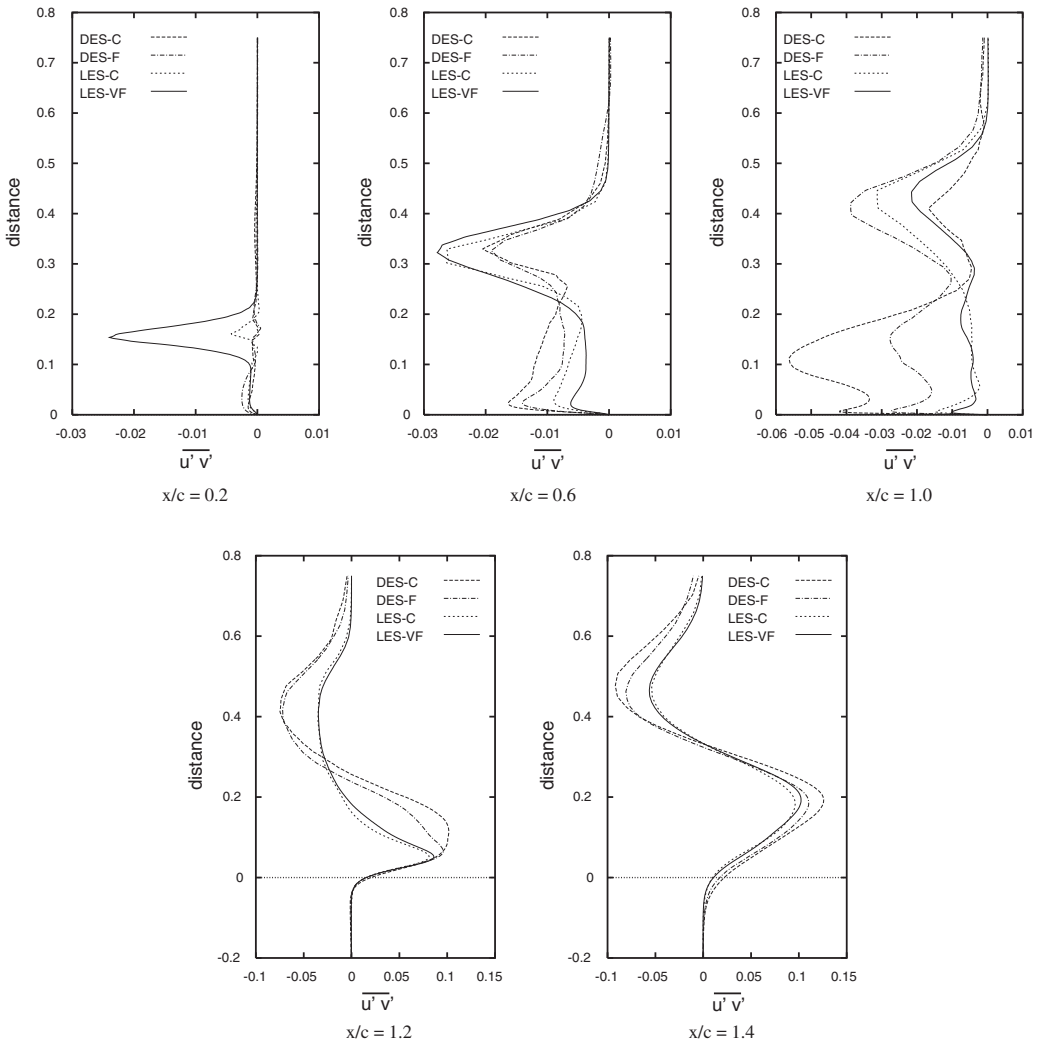

Figure 11. Profiles of the resolved Reynolds stress component $\overline{u'v'}$ as a function of the wall-normal distance at five different locations. $Re_c = 20\,000$ and $\alpha = 18^\circ$.

adequately. A completely different distribution of the eddy viscosity is given by the RANS simulation. Extremely large values of $\nu_T/\nu|_{\max} \approx 368$, especially in the trailing-edge region, are predicted leading to a steady-state result for this highly unsteady flow configuration. This is not surprising, since the RANS approach is not expected to capture the unsteadiness. However, it is interesting to see that the eddy viscosity values are two orders of magnitude larger than in the LES predictions. In contrast, the DES approach aims at a reasonable prediction of the unsteady motion of large-scale structures in a similar manner to LES. As can be seen in Figure 12, both DES cases exhibit similarly very high eddy viscosities in the leading-edge shear layer ($\nu_T/\nu \approx 20$). The shear layer at the trailing edge is also visible by slightly aug-

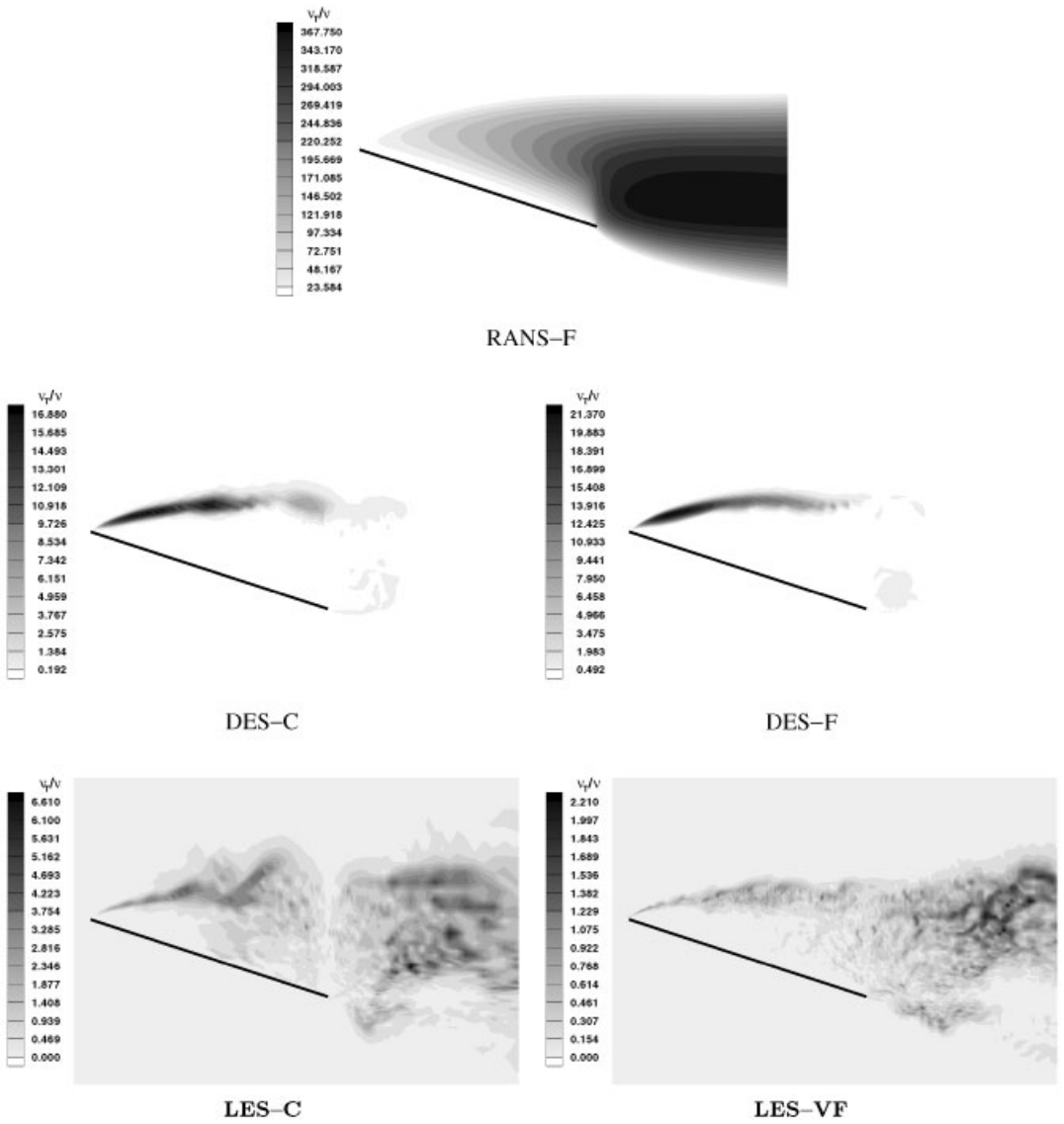

Figure 12. Contours of the eddy viscosity ν_T based on the molecular viscosity ν for the five different simulations defined in Table I. $Re_c = 20\,000$ and $\alpha = 18^\circ$.

mented values of the eddy viscosity, but they are an order of magnitude smaller than the corresponding values in the leading-edge shear layer.

In order to understand this phenomenon, the terms in the eddy viscosity transport equation (5) assumed to be causally responsible for the differences are analysed in more detail. As a matter of principle, the two DES cases do not differ significantly. Therefore, this analysis is restricted to the DES-C case. Since the grids for DES-C and LES-C are in fact the same, this

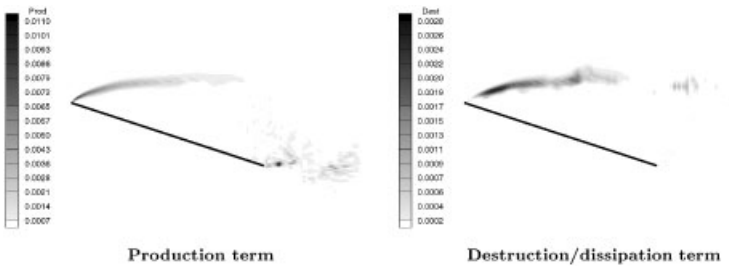

Figure 13. Contours of the production and destruction/dissipation terms computed within the transport equation (5) of the S–A model, DES-C case. $Re_c = 20\,000$ and $\alpha = 18^\circ$.

procedure allows one to draw sound conclusions from the differences of both cases. Figure 13 represents the contours of the production ($c_{b1}\tilde{S}_v\tilde{\nu}$) and destruction/dissipation ($c_{w1}f_w[\tilde{\nu}/\tilde{d}]^2$) terms, respectively, computed as part of the additional transport equation (5) of the S–A model. It is clearly evident that both terms are extremely large in the free shear layer and almost negligible for the rest of the flow domain. This leads to the high eddy viscosity values observed in the shear layer. As will be shown in the following, several issues are responsible for this behaviour of the model.

Postulating a local equilibrium between production and destruction/dissipation in the LES mode of the DES prediction leads to the already mentioned relation $\tilde{\nu} \sim \tilde{S}_v\tilde{d}^2$. In order to convert this relation to the analogue known from the Smagorinsky model, e.g.

$$\nu_T = \mathcal{C} \cdot \mathcal{S} \cdot \Delta^2 \tag{12}$$

the following conditions have to be satisfied in Equations (5)–(8):

$$\begin{aligned} f_{v1} &= 1 \\ f_{v2} &= 0 \\ f_w &= 1 \end{aligned} \tag{13}$$

All three functions were included in the original S–A model (RANS) to take the near-wall region for finite Reynolds numbers correctly into account. In the pure RANS mode the denominator d^2 in Equations (5), (6) and (8) ensures that the importance of the functions (e.g. f_w and f_{v2}) decreases far away from the wall. However, applying the S–A model as a subgrid scale model by replacing d by $\tilde{d}$, this automatism does not work properly, leading to unattended distributions of ν_T/ν as shown in Figure 12. Consequently, in a first step the functions f_{v1}, f_{v2} and f_w were set in accordance to Equation (13) for the LES mode ($\tilde{d} = C_{\mathrm{DES}} \cdot \Delta$) in the DES predictions, which is basically equivalent to the high-Re formulation of the S–A model for the region far away from the wall. This modification already leads to a reduction of the maximum eddy viscosity values of about 100%, i.e. $\nu_T/\nu|_{\max} \approx 10$.

Compared with the LES prediction on the same grid, the DES calculation still leads to much higher values of ν_T. Under the simplifying assumptions mentioned above, the eddy viscosity for both DES and LES can be expressed by Equation (12) for a region far away from any wall, e.g. in the free shear layer. Thus three influencing parameters exist which

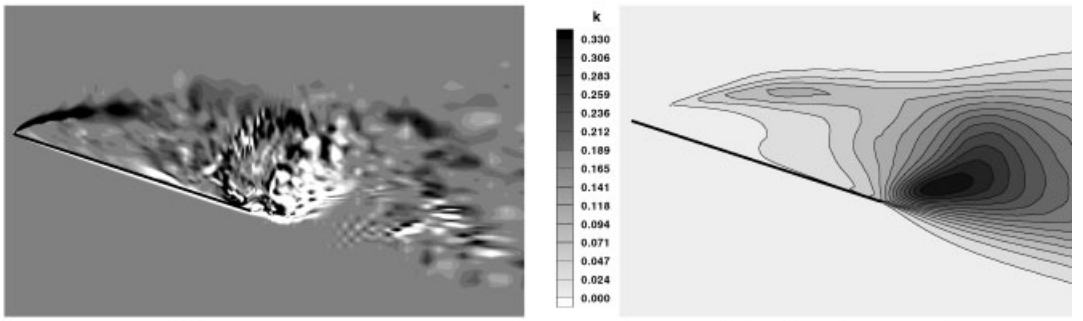

Figure 14. Contours of the vorticity component ω_z of the instantaneous flow field and the distribution of the turbulent kinetic energy k, new DES-C' case. $Re_c = 20\,000$ and $\alpha = 18°$.

may be responsible for the deviations between DES and LES. First the influence of slightly different definitions of $\mathcal{S}$ (LES, $\mathcal{S} = |\bar{S}_{ij}|$; DES, $\mathcal{S} = |\boldsymbol{\omega}|$) was analysed and showed that this difference is not responsible for the large discrepancies between DES and LES. As a second issue the constants $\mathcal{C}$ in Equation (12) were compared, which are given by

$$\mathcal{C} = C_S^2 \quad \text{for LES}$$

and

$$\mathcal{C} = \frac{C_{B1}}{C_{W1}} C_{\text{DES}}^2 \quad \text{for DES}$$

and hence are only slightly higher in the DES case. Consequently, the different definitions of the filter width have to play the most important role for the large deviations occurring between DES and LES. The filter width for DES is based on the maximum grid distance in any direction, whereas LES uses the cube root of $(\Delta x \cdot \Delta y \cdot \Delta z)$. This introduces a factor of about 1.25–4 in favour of the DES filter width in the region of interest. Because the eddy viscosity is proportional to the square of the filter width Δ, large deviations between the predicted values of v_T for DES and LES can be explained.

In order to prove this statement, an additional DES prediction denoted DES-C' was carried out, which differs from DES-C concerning two issues. The first is the conditions for the LES mode defined by Equation (13); the second is a modified filter formulation, where in the original LES region of the DES (i.e. Equation (9) defining the switch between RANS and LES, is not modified) the same definition of the filter width was chosen as for the Smagorinsky model. The investigation clearly shows that this deviation between the two models is mainly responsible for the remaining discrepancies in the results (DES-C versus LES-C). Looking again at the contours of the vorticity component ω_z obtained from the additional simulation (DES-C') shown in Figure 14, a strong improvement is clearly visible. Compared with the original DES-C result, the shear layer is now reproduced more distinctly. Therefore, the roll-up of single eddies in this shear layer is resolved in a similar manner as in the LES-C case.

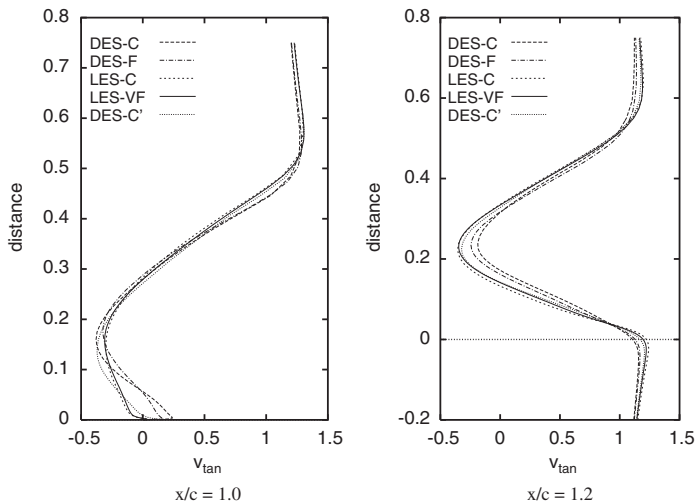

Figure 15. Profiles of the tangential velocities of the averaged flow field as a function of the wall-normal distance at two different locations, new DES-C' case in comparison with previous results. $Re_c = 20\,000$ and $\alpha = 18°$.

Regarding the distribution of the eddy viscosity with respect to the molecular viscosity (not shown here), the latest DES results (DES-C') yield a maximum value of $v_T/v|_{\max} \approx 3.45$ in the free shear layer. As a result of the DES modifications, the previously obtained large discrepancies in the viscosity distribution with reference to the LES cases were reduced to a more reasonable value. Hence the revised formulation of the DES allows more detailed flow structures to be captured. This is also evident in the distribution of the turbulent kinetic energy depicted in Figure 14. In DES-C' the shear layer is now equally well reflected by higher values of k as in the case for LES-C. However, in addition a local maximum of the turbulent kinetic energy is found there which resembles the reference simulation (LES-VF). The deviation of the maximum value of k from the reference value also decreases to a great extent, i.e. from 39% (DES-C) overestimation to 7.5% for the new case (DES-C').

In order to demonstrate also the quantitative improvements obtained from the revised DES formulation, again profiles of the tangential velocity and the Reynolds stress components $\overline{u'u'}$, $\overline{v'v'}$, and $\overline{u'v'}$ at different locations are evaluated. The new results of the DES-C' calculation at two different locations, one at the end of the plate and the other in the wake, are presented in Figures 15 and 16 together with the previous results. A large qualitative and quantitative enhancement with respect to the reference case is found for the tangential velocity and all stress components at all locations evaluated. This is especially noticeable in the $\overline{u'u'}$ component. Whereas the calculations based on the original DES formulation (DES-C, DES-F) exhibit large quantitative deviations from the reference solution, DES-C' reveals good agreement with both LES results. In some plots, e.g. for the $\overline{v'v'}$ and $\overline{u'v'}$ components at $x/c = 1.0$, the DES-C' is partly even closer to LES-VF than LES-C. The overall trend in the distributions of all components at every location is very well captured by DES-C'. This does not hold for the original DES calculations (DES-C, DES-F), for which strong qualitative (and quantitative) deviations in the $\overline{u'v'}$ distribution near the plate and in the wake can be observed.

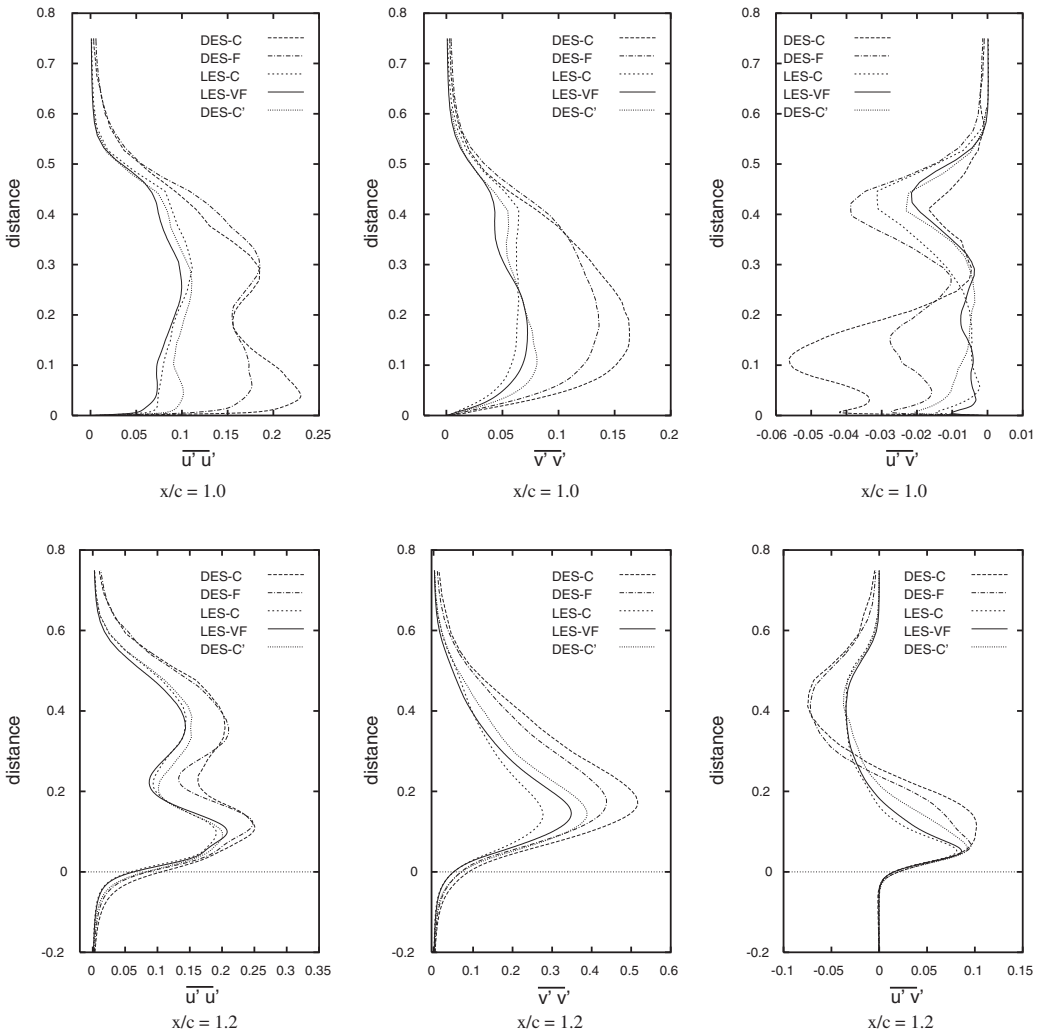

Figure 16. Profiles of the resolved Reynolds stress components $\overline{u'u'}$, $\overline{v'v'}$ and $\overline{u'v'}$ as a function of the wall-normal distance at two different locations, new DES-C' case in comparison with previous results. $Re_c = 20\,000$ and $\alpha = 18°$.

Finally, to complete the scope of comparisons with the previously obtained results, the integral quantities given in Table III are also investigated for DES-C'. Virtually the same value for the mean lift coefficient ($\bar{C}_l = 1.128$) as for the reference case resulted in DES-C'. In addition, almost identical values for the mean drag coefficient ($\bar{C}_d = 0.381$) and the corresponding standard deviations ($\sigma_{C_l} = 6.9 \times 10^{-2}$, $\sigma_{C_d} = 2.1 \times 10^{-2}$) were obtained. The Strouhal number $St = 0.612$ (or $St' = 0.189$) arising from the new DES-C' computation is as close to LES-VF as the DES on the finer grid (DES-F). Therefore, from all the considerations, the modifications applied in DES-C' have led to an overall improvement of the results.

7. CONCLUSIONS

In this investigation, the separated flow past an inclined flat plate ($Re_c = 20\,000$ and $\alpha = 18°$) was computed based on RANS, DES and LES in order to evaluate the quality of the predicted results and especially to reveal the differences between DES and LES. In order to exclude influences from different numerical schemes and different resolutions, all computations were based on the same code and the same grid. In addition, predictions with increased resolution were carried out for all three techniques which allow one to investigate the influence of this aspect. In contrast, no attempt was made to compare the computational resources required for each technique.

As expected, the RANS computations were not able to capture the unsteady vortex shedding behaviour of this bluff-body flow. Both two- and three-dimensional RANS predictions led to the same steady-state results, where no three-dimensional structures were observed in the latter case. In contrast, the asymmetric vortex shedding motion was well reproduced by DES and LES based on different grid resolutions. Concerning the integral parameters, the flow structures and the pressure distribution, the RANS predictions consequently led to the largest deviations with respect to the reference LES solution on a very fine grid (LES-VF). However, comparison of DES and LES predictions carried out on the same grid (i.e. DES-C versus LES-C) yielded considerable differences especially in the representation of the free shear layer and the higher-order statistics. The DES computation (even on the fine grid) was found not to be capable of reproducing the Kelvin–Helmholtz instability adequately. Concerning all relevant flow features, the deviations of both DES computations were always much larger compared with LES-VF than the corresponding LES result on the coarse grid (LES-C). Therefore, this observation was not an effect of the grid resolution but on the modelling of the non-resolved subgrid scales. This is based on the modified S–A model for DES and on the Smagorinsky model for LES. Because the specific test case chosen is favourable to the DES concept and optimal to investigate especially the LES mode of the DES predictions in comparison with pure LES, the determination of the eddy viscosity distribution was analysed in detail. It was shown that two main reasons are responsible for the observed deviations between LES and DES. On the one hand, it was found that special functions included in the S–A model to account for the correct near-wall behaviour of the model do not work properly in the LES mode and have to be excluded from the formulation of the corresponding SGS model. On the other hand, the varying definition of the filter width was identified as being responsible for the remaining large deviations observed in the eddy viscosity levels between the DES and the LES predictions. A revised version of the model for the LES mode taking both issues into account clearly led to strongly improved results (DES-C'). The investigation exhibits that the S–A model can be applied as an SGS model in DES provided that it is properly adapted to this purpose.

ACKNOWLEDGEMENTS

This work was supported by a fellowship from the German Academic Exchange Programme (DAAD) to K. Mazaev, which is gratefully acknowledged. Additionally, the LES contributions were supported by the *Deutsche Forschungsgemeinschaft* under contract number BR 1847/2. The computations were carried out on a variety of high-performance computers. Computing time on the Fujitsu VPP 300 at the RRZE, Erlangen, the Fujitsu VPP 700 at the Leibniz Computing Centre, Munich and the

German Federal Top-Level Compute Server Hitachi SR 8000-F1 at HLRB, Munich are also gratefully acknowledged.

REFERENCES

1. Spalart PR, Jou W-H, Strelets M, Allmaras SR. Comments on the feasibility of LES for wings, and on a hybrid RANS/LES approach, First AFOSR International Conference on DNS/LES, Ruston, LA, 4–8 August 1997. In Advances in DNS/LES, Liu C, Liu Z (eds). Greyden Press: Columbus, OH, 1997.
2. Spalart PR. Trends in turbulence treatments. AIAA Paper 2000-2306, FLUIDS 2000, Computational Fluid Dynamics Symposium: Denver, Colorado, USA, 19–22 June 2000.
3. Spalart PR. Strategies for turbulence modelling and simulations. *International Journal of Heat and Fluid Flow* 2000; **21**:252–263.
4. Speziale CG. Turbulence modeling for time-dependent RANS and VLES: a review. *AIAA Journal* 1996; **36**(2):173–184.
5. Speziale CG. A combined large-eddy simulation and time-dependent RANS capability for high-speed compressible flows. *Journal of Scientific Computation* 1998; **13**:253–274.
6. Germano M. From RANS to DNS: towards a bridging model. In Direct and Large-Eddy Simulation III, Proceedings of the Isaac Newton Institute Symposium/ERCOFTAC Workshop on Direct and Large-Eddy Simulation, Cambridge, U.K., 12–14 May 1999, ERCOFTAC Series, vol. 7, Voke PR, Sandham ND, Kleiser L (eds). Kluwer Academic Publishers: Dordrecht, 1999; 225–236.
7. Shur M, Spalart PR, Strelets M, Travin A. Detached-eddy simulation of an airfoil at high angle of attack, Fourth International Symposium on Engineering Turbulence Modelling and Measurements, Corsica, France, 24–26 May 1999. *Engineering Turbulence Modelling and Experiments*, vol. 4, Rodi W, Laurence D (eds). Elsevier: Amsterdam, 1999; 669–678.
8. Smagorinsky J. General circulation experiments with the primitive equations, I, the basic experiment. *Monthly Weather Review* 1963; **91**:99–165.
9. Spalart PR, Allmaras SR. A one-equation turbulence model for aerodynamic flows. *La Recherche Aérospatiale* 1994; **1**:5–21.
10. Nikitin NV, Nicoud F, Wasistho B, Squires KD, Spalart PR. An approach to wall modeling in large-eddy simulations. *Physics of Fluids* 2000; **12**(7):1629–1632.
11. Forsythe JR, Hoffmann KA, Dietiker JF. Detached-eddy simulation of a supersonic axisymmetric base flow with an unstructured solver. AIAA Paper 2000-2410, *FLUIDS* 2000, Computational Fluid Dynamics Symposium: Denver, Colorado, USA, 19–22 June 2000.
12. Travin A, Shur M, Strelets M, Spalart PR. Detached-eddy simulations past a circular cylinder. *Journal of Flow, Turbulence and Combustion* 2000; **63**(1/4):293–313.
13. Breuer M. A challenging test case for large-eddy simulation: high Reynolds number circular cylinder flow. *International Journal of Heat and Fluid Flow* 2000; **21**(5):648–654.
14. Strelets M. Detached-eddy simulation of massively separated flows. *AIAA Paper* 2001-0879, 2000.
15. Squires KD, Forsythe JR, Spalart PR. Detached-eddy simulation of the separated flow around a forebody cross-section, 4th Workshop on Direct and Large-Eddy Simulation, Enschede, The Netherlands, 18–20 July 2001, ERCOFTAC Series, vol. 8, *Direct and Large-Eddy Simulation IV*, Geurts BJ, Friedrich R, Métais O (eds). Kluwer Academic Publishers: Dordrecht, 2001; 484–500.
16. Breuer M, Jovičić N. Separated flow around a flat plate at high incidence: an LES investigation. *Journal of Turbulence* (http://iop.jot.org) 2001; **2**:1–15.
17. Breuer M, Jovičić N. An LES investigation of the separated flow past an airfoil at high angle of attack. 4th Workshop on Direct and Large-Eddy Simulation, Enschede, The Netherlands, 18–20 July 2001, ERCOFTAC Series, *Direct and Large-Eddy Simulation IV*, vol. 8. Geurts BJ, Friedrich R, Métais O (eds). Kluwer Academic Publishers, Dordrecht, 2001; 165–172.
18. Breuer M, Rodi W. Large-eddy simulation of complex turbulent flows of practical interest. In *Flow Simulation with High-Performance Computers II*, vol. 52. Hirschel EH (ed.), Notes on Numerical Fluid Mechanics, Vieweg: Braunschweig, 1996; 258–274.
19. Breuer M. Large-eddy simulation of the sub-critical flow past a circular cylinder: numerical and modeling aspects. *International Journal for Numerical Methods in Fluids* 1998; **28**:1281–1302.
20. Germano M, Piomelli U, Moin P, Cabot WH. A dynamic subgrid scale eddy viscosity model. *Physics of Fluids A* 1991; **3**(7):1760–1765.
21. Lilly DK. A proposed modification of the Germano subgrid scale closure method. *Physics of Fluids A* 1992; **4**(3):633–635.
22. Kravchenko AG, Moin P. On the effect of numerical errors in large-eddy simulation of turbulent flows. *Journal of Computational Physics* 1997; **131**:310–322.
23. Zhu J. A low-diffusive and oscillation-free convection scheme. *Communications in Applied Numerical Methods* 1991; **7**:225–232.

24. Stone HL. Iterative solution of implicit approximations of multidimensional partial differential equations. *SIAM Journal of Numerical Analysis* 1968; **5**:530–558.
25. Rhie CM, Chow WL. A numerical study of the turbulent flow past an isolated airfoil with trailing edge separation. *AIAA Journal* 1983; **21**:1525–1532.
26. Wille M. Large-eddy simulation of jets in cross flows. *Ph.D. Thesis*, Department of Chemical Engineering, Imperial College of Science, Technology and Medicine: London, U.K., 1997.
27. Lerche Th, Dallmann UCh. Das Prinzipexperiment COSTWING I: Dokumentation der Aufbauphase. Inst. f. Strömungsmechanik, DLR Göttingen, IB 223-99 A04, 1999.
28. Knisely CW. Strouhal numbers of rectangular cylinders at incidence: a review and new data. *Journal of Fluids and Structures* 1990; **4**:371–393.
29. Lam KM. Phase-locked education of vortex shedding in flow past an inclined flat plate. *Physics of Fluids A* 1996; **8**(5):1159–1168.
30. Perry AE, Steiner TR. Large-scale vortex structures in turbulent wakes behind bluff bodies, part 1: vortex formation process. *Journal of Fluid Mechanics* 1987; **174**:233–270.
31. Rodi W, Ferziger JH, Breuer M, Pourquié M. Status of large-eddy simulation: results of a workshop. Workshop on LES of Flows Past Bluff Bodies, Rottach-Egern, Tegernsee, Germany, 26–28 June 1995. *Journal of Fluids Engineering* 1997; **119**(2):248–262.

